Title
Dual-beam optical fiber trapping platform for biophotonics applications

Author
Piñón, Tessa M.

Publication Date
2009

Peer reviewed|Thesis/dissertation

University of California, Merced

Dual-Beam Optical Fiber Trapping Platform for Biophotonics Applications

Submitted for the degree Master of Science

Biological Engineering and Small-Scale Technologies (BEST) graduate program

By

Tessa M. Piñón

August 2009

Abstract

Optical fiber trapping is a technique utilized for manipulating micron-sized dielectric particles such as microspheres and biological cells. In this project we describe the fabrication and particle trapping performance of a compact and inexpensive optical trapping system. The system is constructed using one or more pairs of single-mode optical fibers arranged in a counter-propagating configuration with a small space between the cleaved fiber ends. Particles are trapped by a combination of optical scattering and optical gradient forces from a 980 nm laser, where proper alignment of the fibers is essential for stable performance. Uniform fiber alignment channels are burned into cast acrylic "plexiglass" using resistive wire. The optical fibers are introduced from the sides, stabilized using alignment rods, and glued into place. Observing the system through a microscope and monitoring laser light coupled through the trapping space verifies proper alignment. The resulting system can be scaled to support numerous independent optical traps, and it is small enough to fit into a standard microscope for trapped particle observation.

We investigate the light force dynamics acting on polystyrene microspheres in such a counter-propagating beam trap. Polystyrene particle measurements are a necessary foundation for future studies involving optical cell manipulation and sorting within a microlaboratory environment. To characterize the trapping forces of the system, we modulate the optical power in the trap in order to displace the microsphere from its equilibrium position. The subsequent motion of the particle allows us to calculate the effective spring constant of the trap from which trapping forces can be estimated. We observe spring constants in the range from 100-500 nN/m and forces of 9-60 pN. As an extension of this work, we have scaled the system into a multi-fiber

array of traps. This project sets the stage for simple and consumable microfluidic optical trapping technology.

Acknowledgments

I would like to express my gratitude for the numerous contributions and support that have made my research endeavors possible. I thank my advisor, Dr. Jay Sharping, for his continuous support, patience, and enthusiasm throughout the course of this project. I would also like to thank my thesis committee members, Dr. Carlos Coimbra, Dr. Ariel Escobar, and Dr. Linda Hirst, for their guidance in my research project. My fellow lab members, in particular, Christiane Goulart, Yashwant Verma, Dr. Yan-Hua Zhai, Luis Martinez, Leily Kiani, and Katie Copenhagen, all contributed their lab skills, emotional support, and humor through it all. Special thanks goes to Jeremy Sanborn, "the Mac-to-PC expert," for his tremendous patience and brilliant computer skills to help me navigate any problems I encountered. I want to especially thank the Khine lab and Chin lab for using their laboratory space, chemicals, and cells. Fellow graduate student, Chi-Shuo Chen, was always there to lend a helping hand in the course of my project.

Most importantly, I would like to thank my family and friends for all their continuous love and support throughout the difficult times. Much gratitude goes to my father, Robert, my sisters and brother-in-laws, David and Denise Carrejo and Tony and Jennifer Carrillo, who have all encouraged me and always kept the humor going. Lastly, words cannot explain the amount of emotional support and words of encouragement that my beloved mother, Alicia, gave me to the very end. She continues to be dearly missed. I could not have done it without all the encouragement from my parents, family, and friends for supporting all my educational aspirations.

Table of Contents

List of Figures

Figure **Page**

Figure **Page**

List of Tables

Introduction

Optical trapping was first reported by Ashkin in 1970 and is an optical technique that utilizes radiation pressure from one or more laser beams on a microscopic particle [Ashkin 1970, Ashkin 1987, Constable 1993]. This radiation pressure exerted from laser light induces mechanical forces acting on a particle freely suspended in liquid or air. Micron-sized particles can be trapped in a single beam of light, as in optical tweezers [Ashkin 1986], or in a dual-beam laser trap that permits these particles to be manipulated in three dimensions [Constable 1993, Grover 2001, Kawano 2008, and Lincoln 2007]. Additionally, dual-beam trapping affords a non-contact method to stably hold a single cell or small aggregate [Jess 2006].

In 1970 Arthur Ashkin reports on the first dual beam optical traps comprised of two opposing laser beams focused with lenses [Ashkin 1970]. They trapped freely suspended latex microspheres in water within a glass cell, and later trapped particles in a gas [Ashkin 1970]. They observed that particles wandering near an incident laser beam are drawn in, and accelerate to a stable equilibrium point until coming to a stop when trapped [Ashkin 1970]. Ashkin's initial experiments motivated fundamental insights about radiation pressure behavior and the existence of stable electrical potential wells in the trapping region.

Sixteen years later Ashkin develops the first single-beam optical trapping system for trapping dielectric microspheres in water [Ashkin 1986]. This system is comprised of a strongly focused beam exerting a powerful gradient force that is proportional to the beam intensity gradient [Ashkin 1986]. Ashkin demonstrates successful trapping of dielectric particles ranging from ~25 nm to 10 μm in size [Ashkin 1986].

In 1993, Constable, *et al.* report on a dual-beam optical fiber trapping set-up in which two fibers are well aligned and oppose one another [Constable 1993]. Constable, *et al.* [1993] trap

polysytrene spheres of diameters ranging from 0.1 μm to 10 μm with single-mode fibers placed into alignment using simple, inexpensive laboratory materials to form a small trapping cell space. One trapping scheme involves two pigtailed diode lasers, one with a wavelength of 1.3 μm and the other with wavelength of 0.831 μm [Constable 1993].

Fig. 1.

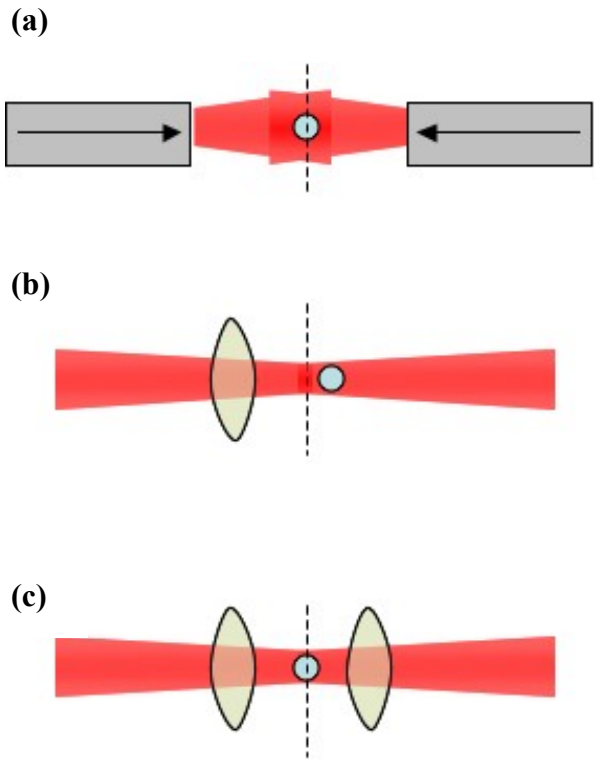

Fig. 1. Schematic of the three most common types of optical traps. **(a)** Dual-beam optical fiber trap with overlapping diverging beams emerging from the counter-propagating fibers. The trapped particle sits in the center of the trapping region (denoted by the dotted line). **(b)** Typical optical tweezer (single beam trap) with a very tightly focused beam. The beam waist is the region of strongest intensity and a high gradient force. A trapped particle sits slightly away from the beam waist due to the scattering force in direction of beam propagation. **(c)** Dual-beam focused trap with two opposing beams that are tightly focused. The trapped particle sits in the beam waist.

Design considerations

Dual-beam optical trapping offers distinguishable benefits compared to other trapping techniques (see Fig. 1). In contrast to dual-beam trapping, optical tweezers utilizes the gradient force in all three dimensions for trapping particles formed by a tightly focused beam [Ashkin 1986]. In order to achieve gradient force trapping with a single beam in three dimensions, one must use a tightly focused beam, and therefore, optical intensity is typically high in the trapping

region [Grover 2001]. Special care must be taken to insure cell viability since factors such as intensity, wavelength, and time span of exposure correlate to viability [Neuman 1999]. Viability of *E. coli* bacterial cells in optical tweezers have been investigated in the near-infrared range of λ = 790-1064 nm with continuous-wave (CW) lasers, with λ = 970 nm exhibiting the least damage (followed closely by 830 nm) on the cells [Neuman 1999 and Mirsaidov 2008]. Mirsaidov, *et al.* [2008] also perform viability assays on *E. coli* and find λ = 900 nm causes the least photodamage. They indicate that cell viability in CW traps depends little on wavelength, but rather depends on peak power, suggesting a detrimental threshold of energy (5 J) for *E. coli* [Mirsaidov 2008].

The absorption coefficient for water is a function of wavelength [Jonasz and Fournier 2007]. For wavelengths ranging from 380 nm to 2.5 μm, our wavelength λ = 980 nm (or 10, 200 cm^{-1}) exhibits moderate absorption at 22°C with an absorption coefficient of 9 m^{-1} [Jonasz and Fournier 2007]. Due to the high water content of biological cells, this is an essential factor for us to consider when we pursue biological cell applications.

In comparison to other trapping schemes, the approach of Constable highlights some advantages of the dual-beam optical trap: 1) microscope viewing of trapped particles is conducted in a different plane from trapping; 2) no external optics are required for focusing beams; and 3) trapping is conducted with readily available continuous-wave diode lasers and alignment method utilizes inexpensive, consumable materials. Constable [1993] also mentions success with trapping living yeast, which at time, biological uses of optical trapping were only beginning.

Applications

Much attention has been drawn to the vast biological applications of optical trapping. Optical trapping has been used as a tool to measure piconewton-range forces in a variety of biological processes [Constable 1993, Ghosh 2006, and Prasad 2003] and for cell sorting applications [Applegate 2006 and Grover 2001]. More recently there is interest in developing practical, miniature cell particle sorting microfluidic platforms for medical diagnostics [Wang 2005, Applegate 2006, Grover 2001]. Conventional fluorescent activated cell sorting (FACS) and flow cytometry techniques necessitate cumbersome instrumentation, and are not readily available for micro-scale studies [Applegate 2006]. Typical large-scale cell population instrumentation techniques often average readouts detailing information about groups of cells, often neglecting the dynamic behavior of individual cells within a large group [Eriksson 2007].

Recently, the dual-beam trapping technique has been coupled with other tools such as Raman spectroscopy that provides chemical-specific information without the need for protein labeling [Jess 2006]. Jess, *et al.* have shown the implications of using a dual-fiber trap to record Raman spectra for large cells (human keratinocytes, human promyelocytic leukemia, and human cervical squamous carcima cells) and local parts of these cells to differentiate these various cell types [Jess 2006]. Chan, *et al.* [2009] have employed Raman spectroscopy to biochemically differentiate human embryonic stem cells (hESCs), human fetal left ventricular CMs, and hESC-CMs, with up to 98% accuracy for human fetal CMs.

Another method for single-cell interrogation is total internal reflection fluorescence (TIRF) microscopy in combination with optical tweezers [Snijder-Van As 2009]. In this study binding dynamics of ALCAM-GFP (activated leukocyte cell adhesion molecule with green fluorescent protein tag) with its ligand CD6 immobilized onto a surface are investigated

[Snijder-Van As 2009]. Here the TIRF-Optical tweezers combination exemplifies a method to precisely control the timing and position of cell-substrate interactions to study key cell communication responses [Snijder-Van As 2009]. Since optical trapping affords good temporal and spatial control of cells, we may utilize our trapping system to study embryonic stem cell aggregates of precisely controlled sizes and study the role of cell-cell communication among aggregates that mediates differentiation [Park 2007]. Additionally, we aim to incorporate our optical system into a microfluidic system. Optical trapping combined with microfluidic devices realizes the ability to mimic cell-environment and cell-cell interactions that are present *in vivo* [Cran-McGreehin 2006, Enger 2004, and Lincoln 2007].

The current trend in microfluidics is leaning toward flexible and rapid processing techniques in order to meet the demands of rapid turn-around time and to lower the cost in developing these products [Malek 2006]. While polydimethylsiloxane (PDMS) is one of the most commonly used materials for constructing biochips due to its biological compatibility and flexible material nature, there is growing interest in fabricating chips from biocompatible, sturdy plastic [Becker 2001]. Plastic chips are less expensive and are more adapted to mass-production techniques than silica-based products [Malek 2006].

Trapping forces and scattering background

A laser beam interacting with a particle such as a dielectric sphere or biological cell exerts two major categories of forces objects such as dielectric spheres or biological cells [Ashkin 1987, Constable 1993, Guck 2005, Lincoln 2007]. The *scattering force*, acts in the direction of beam propagation and it is result of a change in momentum of photons scattering off the surface of the microsphere [Constable 1993, Grover 2001, Kawano 2008]. The other force acting on a trapped particle is the *gradient force* that acts proportional to and in the same

direction as the spatial gradient in light intensity [Constable 1993, Grover 2001, Kawano 2008] (see Fig. 2).

Fig. 2. Schematic describing the concurrent scattering forces from each incident Gaussian beam in the direction of light propagation and two gradient forces perpendicular to light propagation. A trapped spherical particle experiences a net force of zero.

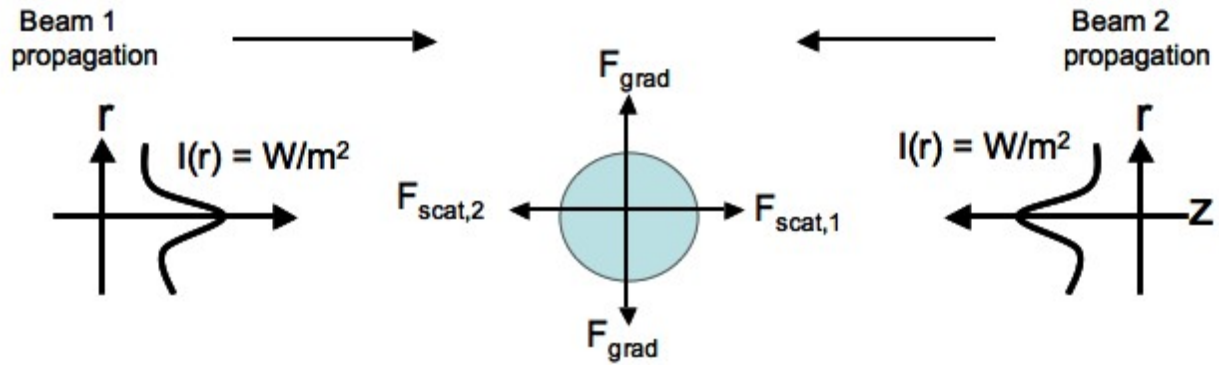

The gradient force arises from the transfer of momentum between photons and the particle as light passes through a transparent or near-transparent object [Constable 1993, Grover 2001, Kawano 2008, Guck 2005]. Photons with a given momentum are refracted through the dielectric object with a given index of refraction greater than that of the outside medium [Grover 2001, Guck 2005]. For this reason, a polystyrene microsphere (of refractive index n = 1.59) optically trapped in water (n = 1.33), acts as a focusing lens for the incident beams [Ashkin 1970]. The change of momentum in the refracted photon causes an equal and opposite change in the momentum of the object, imparting a force on the object equal to the net rate of change of momentum of all refracted photons [Grover 2001, Guck 2005].

When the particle is situated at intersecting divergent laser beams, some of the incident light is refracted as it passes through the particle and the rest is reflected [Constable 1993 and

Grover 2001]. The photons of the refracted light from a particle emerge with a different momentum from the incident momentum, imparting a change of direction for the particle, and creating a net gradient force that pulls the particle to a beam region of increasing intensity [Constable 1993, Grover 2001, Lincoln 2007, Kawano 2008]. On the contrary, the reflected light from the net scattering forces exerts a "pushing force" on the particle in the opposite direction from the light refraction "pulling force" [Constable 1993, Grover 2001, Lincoln 2007, Kawano 2008] (see Fig. 3). The net effect of the two forces is a stable trapping region in the center of the two opposing laser beams [Lincoln 2007]. The net gradient force is of greater magnitude than scattering forces [Lincoln 2007]. Another difference is gradient forces are additive, whereas the opposing scattering forces cancel for a stable trap [Lincoln 2007]. As first demonstrated by Ashkin in 1970, if a beam hits a microsphere off-center, the sphere is restored back into the beam axis and accelerated in the direction of light incidence [Ashkin 1970].

.

Fig. 3. Illustrations of two counter-propagating divergent laser beams with scattering and gradient forces acting on a trapped spherical particle. Forces incident on the particle are depicted by light rays (F_1, F_2, F_3, and F_4) incident on a particle. The forces are integrated over the entire surface, inducing a net force equivalent to 0 when the particle is stably trapped. **(a)** Two opposing optical fibers with diverging overlapping beams depicting the trapping region for a particle. **(b)** Interactions of scattering and gradient forces on a stably trapped spherical particle. The scattering forces cancel one another (net F_{scatt} = 0) and the gradient forces are additive. Refraction vectors (due to gradient force) and reflection vectors (due to scattering forces) are shown. **(c)** Schematic of a spherical particle displaced from center of the trap with gradient force pulling the particle back into the trap.

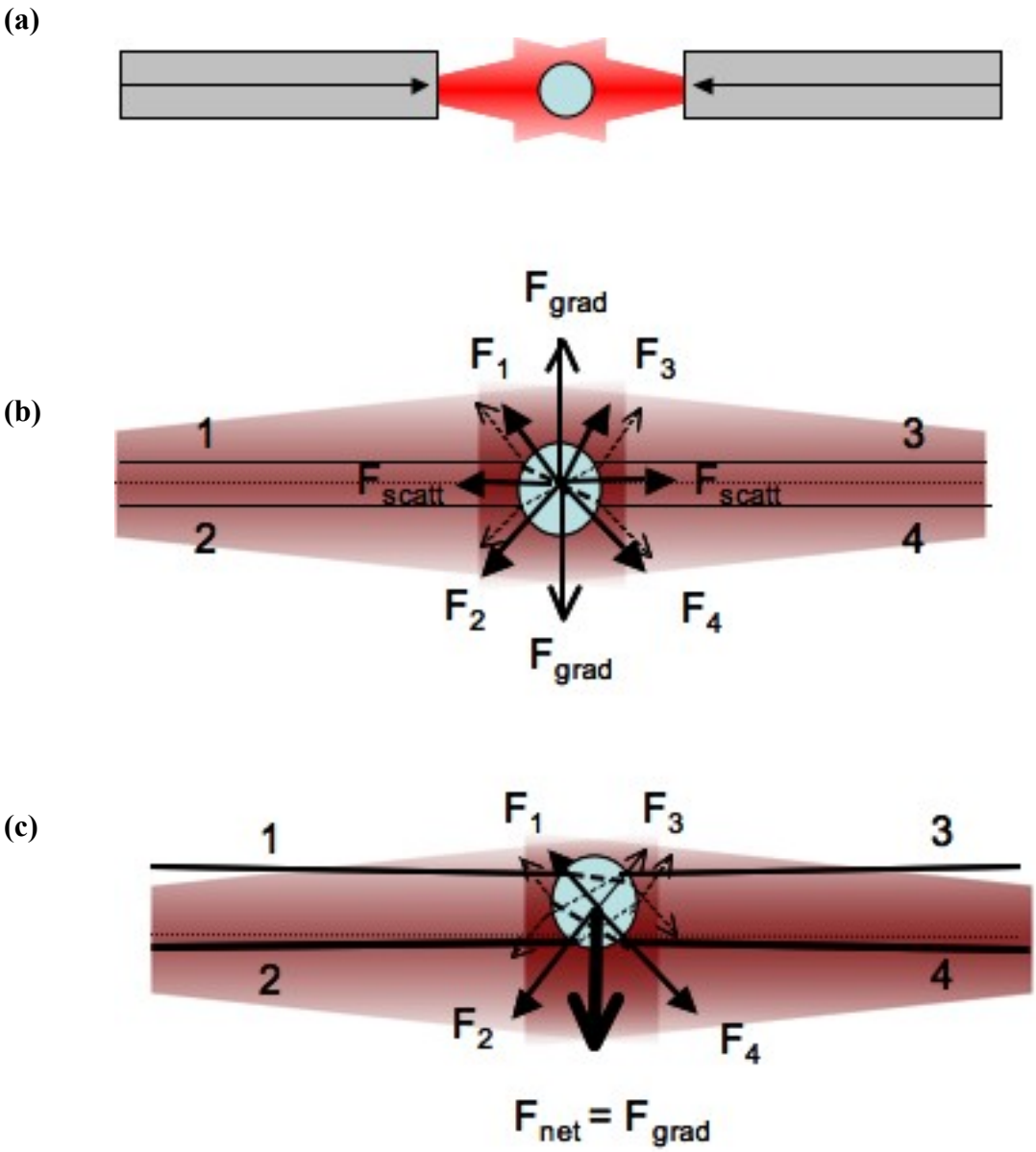

Scattering theory

Before discussing scattering theory and relative mathematical implications, a more qualitative explanation for scattering phenomena will be introduced. When an electromagnetic field illuminates a dielectric particle, electric dipole moments are induced throughout the particle, causing electronic polarizability [Bohren and Huffman 2004, Thomas 2006]. These dipole moments oscillate at an equivalent frequency of the incident field, and emit secondary radiation wavelets in all directions (all angles of θ) [Bohren and Huffman 2004]. The net scattered field is mathematically determined by superposing these scattered wavelets and accounting for phase shift variations [Bohren and Huffman 2004]. Phase relations heavily depend on parameters such as particle material and scattering direction; the geometrical factors of particle size and shape also affect scattering phase behavior [Bohren and Huffman 2004]. Due to the symmetry of the microsphere, the scattered field is independent of incident light polarization state [Bohren and Huffman 2004].

Since the early 1900s, thorough analyses detailing the theory of absorption and scattering by small spherical particles have been demonstrated [Bohren and Huffman 2004]. Among the scientists who worked on the sphere problem were Gustav Mie, Lorenz, and Peter Debye, who all sought to develop mathematical approximations and theories to explain absorption and scattering effects of a spherical particle with an arbitrary radius and refractive index [Bohren and Huffman 2004]. The availability of computers in later years permitted a convenient means to perform detailed computations to explain the complex physical interaction of an electromagnetic wave with a sphere. Although involved explanations of these rigorous calculations are beyond the scope of this thesis project, expressions for absorption and scattering cross sections will be discussed as well as the methods used for calculating Mie scattering coefficients for this project.

Our system parameters satisfy Mie scattering conditions for the wavelength (λ = 980 nm) and microsphere sizes (d = 6 μm and 10 μm) we employ. Details about Mie particle scattering dynamics for our system will be discussed later. In brief, the Mie scattering regime is satisfied for particle sizes larger than the incident wavelength, and when these particles are optically trapped, the gradient force tends to draw objects toward regions of greater light intensity [Constable 1993, Grover 2001, Guck 2005].

Light carries both momentum and energy in the direction of its propagation due to photons acting as a continuous stream of particles [Bohren and Huffman 2004]. Thus, incident light exerts a force on a scattering particle called radiation pressure [Van de Hulst 1981, Bohren and Huffman 2004]. For incident light with a certain intensity I_o on an isotropic particle of a cross sectional area $G = \pi a^2$, the force acting on the particle due to radiation pressure is $F = I_o(G/c)Q_{pr}$, where c is the velocity of light [Van de Hulst 1981]. Q_{pr} is defined as the efficiency factor for radiation pressure which is a ratio defining the transfer of momentum to particle from the initial electromagnetic radiation momentum [Van de Hulst 1981, Bohren and Huffman 2004].

Spherical particles of geometrical cross section G scatter light equivalent to that of incident light on an area GQ_{sca} and can partially absorb incident radiation on an area GQ_{abs}, where Q_{sca} and Q_{abs} are scattering and absorption coefficients, respectively [Burns 1979, Van de Hulst 1981]. These coefficients depend on radiation wavelength and relate to energy scattered and absorbed by the particle. The relationship among the efficiency factors for extinction, scattering, and absorption is summarized as: $Q_{ext} = Q_{sca} + Q_{abs}$ [Van de Hulst 1981]. Fully absorbing particles have $Q_{ext} \neq Q_{sca}$ [Van de Hulst 1981] and $Q_{pr} = Q_{abs} = 1$ [Burns 1979]. Complete transmission (i.e. no particle, $Q_{trans} = 1$) occurs when $Q_{pr} = 0$, whereas total absorption is equivalent to $Q_{pr} = 1$ [Burns 1979].

For non-absorbing spheres, $Q_{pr} = 1 - g$, where g is the asymmetry parameter defined as <cos θ>, a weighted average of scattering angles θ due to elastic scattering occurring at some distribution of angles [Bohren and Huffman 2004, Van de Hulst 1981, Irvine 1965]. As stated by Irvine [1965], the asymmetry factor characterizes forward-to-backward scattering from a particle. In cases of isotropic scattering (i.e. uniform scattering in all directions), <cos θ> = 0 [Bohren and Huffman 2004, Shah 1991]. The asymmetry parameter <cos θ> also equals zero when scattering occurs perpendicular ($\theta = \pm 90°$) to the direction of incident radiation ($\theta = 0°$) [Shah 1991]. A dominant forward scattering ($\theta = 0°$) insinuates a positive asymmetry parameter, whereas a dominant back scattering ($\theta = 180°$) defines a negative asymmetry parameter value [Bohren and Huffman 2004]. Values of Q_{pr} and <cos θ> are related to the normalized scattering and extinction cross sections Q_{sca} and Q_{ext} by $Q_{pr} = Q_{ext} - <\cos\theta> Q_{sca}$ [Irvine 1965].

The total momentum transfer due to radiation pressure acting on a trapped particle must be conserved [Bohren and Huffman 2004]. A scattered beam exerts a forward momentum equivalent to Q_{sca} <cos θ> in the forward direction [Burns 1979]. Since diffraction does not contribute to momentum transfer for a particle, the phenomenon of scattered radiation is defined by $Q_{sca} + Q_{abs} + Q_{trans} = 1$ [Burns 1979].

The complex index of refraction is defined as $m = m' + im''$ where m' is the real refractive index for phase velocity, im'' indicates the imaginary refractive index component [Bohren and Huffman 2004, Mätzler 2002]. The refractive index ratio, m, is equivalent to N_1/N, the refractive index of the particle relative to the surrounding medium [Bohren and Huffman 2004]. This research project assesses spheres of non-absorbing (dielectric) material, meaning the sphere is not electrically conductive and the refractive index ratio, m, of the material is a real constant as discussed by Van de Hulst [1981]. A real value of m indicates *no* absorption, so we know

beforehand that $Q_{sca} = Q_{ext}$. In contrast, for absorbing particles, $Q_{sca} \neq Q_{ext}$ [Van de Hulst 1981]. In this experiment, plain micron-sized polystyrene spheres have a real refractive index of 1.59 and are assumed to be non-absorbing.

In a physical sense, the linearly polarized plane wave scattering process from a sphere and all encompassing electromagnetic wave interactions are interpreted with mathematical approximations. In order to accurately approximate scattering amplitude and phases, it is important to identify the correct scattering model for calculation purposes. Rayleigh scattering and Mie scattering are the most general scattering regimes. Both of these regimes have different experimental assumptions, including particle size-to-wavelength boundary conditions and media refractive indexes to be utilized in an experiment [Van de Hulst 1981]. As explained by Van de Hulst [1981], when considering the rigorous formulae of scattering theory, three limiting size parameters are fundamental for the theoretical *m-x* scattering domains, where $x = 2\pi a/\lambda$, a is the particle radius, and λ is defined as incident wavelength: 1) the size of the scattering sphere, x, can have values ranging from 0 to ∞, with scattering patterns gradually changing for smaller spheres to larger spheres; 2) the refractive index, m, which can have values between 1 and ∞, (when $m = \infty$, particle is total reflector); and 3) *phase shifts* of a light ray passing through the sphere along its diameter is $2a \cdot (m - 1) \cdot 2\pi/\lambda = 2x(m - 1)$. As discussed by Van de Hulst, there are six boundary regions in the *m-x* domain that inherently approximate scattering behavior [1981].

The first scattering domain is the Rayleigh regime that holds true for particles of small size (i.e. atoms and small molecules) in comparison to the applied wavelength [Thomas 2006]. Some fundamental conditions for the Rayleigh regime are: $|m - 1| << 1$ *and* $2x|m - 1| << 1$ [Van de Hulst 1981]. Rayleigh scattering has greater forward scattering than backscattering [Van

de Hulst 1981]. Particles experiencing Rayleigh scattering (i.e. small x values) produce secondary wavelets with minimal phase shift [Bohren and Huffman 2004]. A central incident ray coming into contact with the sphere undergoes a phase lag, ρ, after passing through the sphere due to the refractive index boundary (e.g. water to polystyrene material) [Van de Hulst 1981, Jonasz and Fournier 2007]. The phase shift is expressed as $\rho = 2x\ (m - 1)$ [Van de Hulst 1981] and typically the condition $\rho < 0.3$ holds true for Rayleigh scattering [Barth 1984]. While smaller particles exhibit less scattering intensity and have characteristically large scattering angles, larger particles scatter greater amounts of radiation with smaller angles [Barth 1984].

In contrast to Rayleigh particles, larger particles (compared to incident wavelength) scatter wavelets that undergo constructive and destructive interference [Bohren and Huffman 2004]. The Mie scattering regime generally holds true as particle size increases from 1/10 to 10 times the incident wavelength [Barth 1984], where $x >> 1$ [Van de Hulst 1981]. The Mie scattering theory is a general solution to Maxwell's equations for spherical particles of arbitrary size and refractive index [Thomas 2006]. Other fundamental characteristics for Mie scattering are highly pronounced changes in phase shift [Van de Hulst 1981], where $\rho \approx 1$ satisfies Mie scattering conditions [Barth 1984].

The Mie theory more thoroughly describes the absorption and scattering modes of electromagnetic waves interacting with a sphere [Bohren and Huffman 2004]. Scattered waves from a homogenous dielectric spherical particle are described as a superposition of normal electromagnetic modes for spherical harmonics, each denoted by the coefficients a_n or b_n which represent two of four linear simultaneous equations [Bohren and Huffman 2004]. The other two Mie coefficiencts, c_n and d_n, relate to the electromagnetic field inside the incident particle [Bohren and Huffman 2004]. Refer to Bohren and Huffman [2004] for a detailed overview of

these four coefficients. The scattering coefficients a_n and b_n are important quantities to determine, since other values including efficiency cross section terms and scattering matrix elements can be directly solved from these coefficients [Bohren and Huffman 2004].

For our experimental investigation we calculate the phase shift, ρ, for our trapped polystyrene microspheres with size parameters x = 19.2 (sphere radius = 3 μm) and x = 32.1 (sphere radius 5 μm): ρ = 7.7 (for x = 19.2) and ρ = 12.8 (for x = 32.1). This indicates ρ directly correlates to microsphere size; that is, more scattering phase interference is generally present. Phase shift condition limits do not denote exact scattering regime transitions—rather, they provide guidelines for when these regimes are applicable [Barth 1984]. Furthermore, our particle size parameters in comparison to the incident wavelength (λ = 980 nm) are considered to be intermediately large according to regime standards described by Van de Hulst [1981]. For this optical trapping investigation, two microsphere sizes with radius a = 3 μm and = 5 μm are trapped with infrared light with λ = 980 nm. When calculating the size-wavelength parameter, x, for our experiment, we arrive at x = 19.2 and x = 32.1 for the 3 μm and 5 μm particle sizes, respectively. Although Mie theory is typically for "very large" spherical particles such that $x >> 1$, after careful study of various scattering regimes and their conditions, we conclude that the Mie theory most closely appropriates the scattering behavior of our optical trapping system.

Furthermore, our particle material, polystyrene, has a refractive index of 1.59, which follows the assumption for m values very close to 1. Our trapping experiments are conducted in water (n = 1.33), which cause the incident optical rays to cross a water-polystyrene boundary with two different refractive indexes. As a result, the optical rays refract, or internally bend, toward the optical normal through the sphere. Since the refractive index ratio of polystyrene to water (m = 1.2) is just above unity value of 1, incident rays experience little deviation at the

media boundary [Van de Hulst 1981]. Geometrical ray optics explains these ray interactions within the sphere, including refraction [Van de Hulst 1981].

Mätzler's Mie coefficient MATLAB programs [2002] have been quite beneficial in our project to accurately calculate scattering efficiency factors, including the most relevant, Q_{pr}, the efficiency factor for radiation pressure. The factor Q_{pr} is defined in the spring constant expression (Eqn. 1) and scattering force expression (Eqn. 2) both of which will be calculated and discussed in later detail. Mätzler's MATLAB programs are heavily based on quantum mechanics and electromagnetic theory for particle scattering theory. These MATLAB programs contain supplementary material that summarizes some of the most referenced textbooks in particle scattering theory, including those of Van de Hulst [1981] and Bohren and Huffman [2004]. Furthermore, Mätzler includes comments in most sections of his MATLAB program code that often reference page numbers in Bohren and Huffman's textbook. We will demonstrate how Mätzler's Mie scattering coefficient MATLAB program accurately determines the efficiency cross sections Q_{ext}, Q_{sca}, Q_{abs}, Q_{pr}, and the asymmetery parameter $< \cos \theta >$.

Although we conducted minor modifications to Mätzler's original set of programs for ease of use, we have verified the validity of these modified programs by arbitrarily reproducing different extinction curves based on Mie's formulae found in Irvine's article [1965] and Van de Hulst's textbook. In Fig. 4, we have reproduced efficiency curves using stated parameters utilized to plot extinction curves in Irvine's article [1965, Fig. 1 in article]. By comparing the extinction curve plots, we can see that Mätzler's program accurately calculates efficiency factors.

Fig. 4. Here we use Mätzler's MATLAB Program to plot Mie scattering curves. We have tested the accuracy of Mätzler's program by reproducing curves from Irvine [1965, Fig. 1 in the article] of extinction coefficient Q_{ext}, asymmetry factor <cos θ>, and radiation pressure coefficient Q_{pr} for dielectric spheres with m = 1.20. Calculations conducted for size parameter x = 0.5 to 30. Our reproduced plot of the coefficient curves created on MATLAB is shown below.

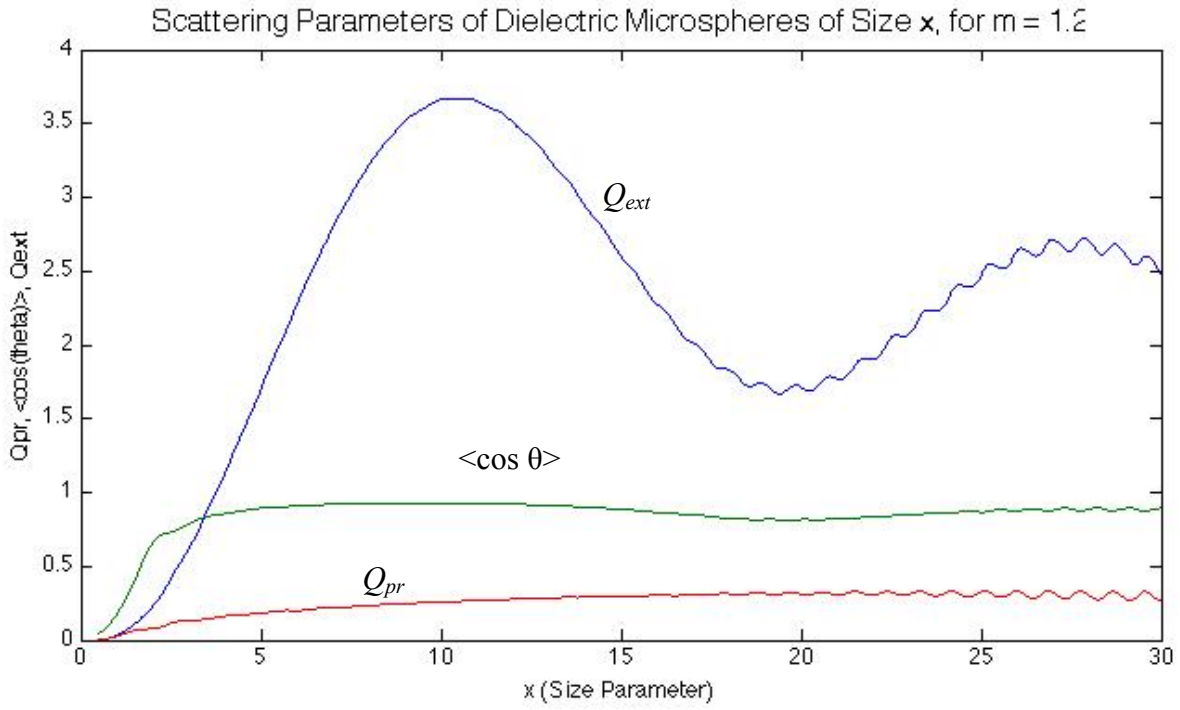

Once the MATLAB particle tracking is complete, the data comprised of pixel position and time stamps are uploaded into IGOR PRO software for curve fitting and further analysis of time constants. As previously explained in the experimental methods section, the time constant is used to calculate spring constant values for both increase and decrease exponential curves. One term in the spring constant expression (Eqn. 1) and scattering force expression (Eqn. 2), radiation pressure efficiency coefficient, Q_{pr}, is calculated with Mätzler's Mie scattering coefficient MATLAB program. After input of experimental parameters into the program (sphere radius, surrounding medium refractive index, particle refractive index, and incident wavelength), an algorithm returns all Mie scattering efficiencies calculated from a matrix of the four scattering

coefficients: a_n, b_n, c_n, and d_n with infinite n series from $n = 1$ truncated to $nmax = x + 4x^{1/3} + 2$ (proposed by Bohren and Huffman 2004), where x is the size-wavelength parameter (see Fig. 5). Refer to Appendix for Mie scattering coefficient program.

Fig. 5. Mätzler's Mie scattering MATLAB program is utilized to calculate the radiation pressure coefficient Q_{pr}. Here we show the scattering efficiencies and Mie coefficients we calculate for our trapping experiment of polystyrene spheres (d = 6 μm and 10 μm) in water. In addition to Q_{pr}, Mätzler's program returns all other Mie efficiencies: Q_{ext} (extinction), Q_{sca} (scattering), Q_{abs} (absorption), Q_b (backscattering), <cos θ> (asymmetry parameter), Q_b/Q_{sca}, and Q_{pr} (radiation pressure). Mie coefficients a_n, b_n, c_n, d_n are also returned with the infinite series truncated to n_{max} as formulated by Bohren and Huffman (1983). Mie coefficients are returned in a series of matrix columns and rows for each n term, where each row relates to a_n, b_n, c_n, and d_n in sequential order. Columns refer to coefficient groups for each n term. We have shown coefficients for the first three n terms only. **(a)** Mie scattering calculations for plain polystyrene microsphere d = 6 μm. **(b)** Mie scattering calculations for plain polystyrene microsphere d = 10 μm.

(a)

```
EDU>> tessamie_abcd6um
For 6.0um diameter dielectric polystyrene microsphere
     Qext        Qsca        Qabs     Qb    <cos(theta)> Qb/Qsca     Qpr
    2.5199     2.5199          0    0.9922     0.8848     0.3938     0.2902


ans =

  Columns 1 through 3

   0.8686 + 0.3378i   0.9677 + 0.1769i   0.8941 + 0.3078i
   0.9631 + 0.1886i   0.8775 + 0.3279i   0.9742 + 0.1586i
   0.2079 - 1.0616i   0.3763 - 1.0071i   0.1791 - 1.0995i
   0.3942 - 1.0138i   0.1968 - 1.0767i   0.3445 - 1.0007i
```

(b)

```
EDU>> tessamie_abcd10um
For 10.0um diameter dielectric polystyrene microsphere
     Qext        Qsca        Qabs     Qb    <cos(theta)> Qb/Qsca     Qpr
    2.3764     2.3764    -0.0000    0.6853     0.9153     0.2884     0.2013


ans =

  Columns 1 through 4

   0.8555 + 0.3515i   0.7195 + 0.4492i   0.8698 + 0.3365i   0.7476 + 0.4344i
   0.7122 + 0.4527i   0.8619 + 0.3450i   0.7301 + 0.4439i   0.8803 + 0.3247i
  -0.5882 + 0.9254i  -0.4015 + 1.0033i  -0.5598 + 0.9207i  -0.3833 + 1.0391i
  -0.4080 + 0.9928i  -0.5767 + 0.9236i  -0.3941 + 1.0185i  -0.5343 + 0.9197i
```

Mechanics of trapped particles

Constable's work is a motivation for this project, and has been fundamental for calibrating and characterizing our basic dual-beam optical fiber trapping system. Mathematical approximations for determining the spring constant (κ) and scattering forces will be referenced throughout this work. For incident light on a dielectric sphere of a given area being trapped with two counter-propagating beams the spring constant, κ, is given by:

$$\kappa = 16\pi^2 aS\left[\frac{P_1 Q_{pr,1}\omega_{0,1}{}^2}{\lambda_1{}^2(S^2+4d_1{}^2)^2}+\frac{P_2 Q_{pr,2}\omega_{0,2}{}^2}{\lambda_2{}^2(S^2+4d_2{}^2)^2}\right] \qquad \textbf{(Eqn. 1)}$$

where $a = 2R^2/c$ (the incident geometrical cross-sectional area of the sphere), and R = sphere radius (R = 3 μm and R = 5 μm); c = velocity of light in a vacuum; P = incident power; $d^{-1} = \lambda/(\pi\omega_0{}^2)$, where λ = incident laser wavelength (980 nm) and ω_o = Gaussian beam waist (5 μm); S = fiber separation (typical range 50 μm to 250 μm); Q_{pr} = radiation pressure coefficient which was calculated from C. Mätzler's "MATLAB Functions for Mie Scattering and Absorption" program (2002) to be discussed in detail later.

The equation for the total scattering force acting on a trapped particle is given by:

$$F_s = \frac{aP_1 Q_{pr,1}/\omega_{0,1}{}^2}{1+d_1^{-2}(S/2+z)^2}-\frac{aP_2 Q_{pr,2}/\omega_{0,2}{}^2}{1+d_2^{-2}(S/2-z)^2} \qquad \textbf{(Eqn. 2)}$$

where z is the distance from the center region between the fibers (i.e. z = 0 corresponds to the center point).

An optically trapped microsphere in the dual-beam fiber set-up is a classic example of Hooke's Law *(F = – κΔx)* for springs in classical kinematics, where *F* is the restoring force due to a displacement of a particle from its equilibrium position, Δx. The spring constant, κ, is a measure of stiffness for the optical trap. A trapped microsphere at rest with $\Delta x = 0$ (static equilibrium) will remain at rest (net scattering force = 0). When one of the laser power outputs is changed, the shape and location of the optical trap changes. At that instant there exists an unbalanced force on the trapped microsphere given by Hooke's law where Δx is equal to the shift in the equilibrium position of the optical trap. For example, increasing the output power emerging from the laser on the left results in the equilibrium position of the trap shifting to the right. The stiffness of the trap changes as well. The particle experiences a restoring force that is proportional to the displacement.

The interaction of laser forces propelling a polystyrene sphere through water is modeled as a highly overdamped system [Constable 1993]. The equation of motion is expressed as: $\sum F = m\ddot{x} = -c\dot{x} - \kappa x$. The drag coefficient, *c*, is given by Stokes' Law: $c = 6\pi\mu r$ where μ is the dynamic viscosity of water and *r* is the radius of the sphere [Grover 2001 and Deng 2007]. At the end of the particle's motion, the velocity reaches 0. Over damping conditions are satisfied when the damping parameter *c* is larger than the angular frequency, $\omega_o = \sqrt{\frac{\kappa}{m}}$, where κ is the spring constant and *m* is particle mass [Fowles and Cassidy 2005]. Equivalently, the parameter $\sqrt{\gamma^2 - \omega_o^{\,2}} > 0$, where $\gamma = c/2m$ is satisfied for an overdamped system [Fowles & Cassidy 2005]. The time constant, τ, is determined from the exponential fit of a microsphere's position versus

time plot when it is displaced from equilibrium. The spring constant, κ, is then determined from the following equation: $\kappa = \frac{6\pi\mu r}{\tau}$.

Theoretical plots (Fig. 6) of spring constant as a function of fiber separation for various power output setting highlight the range of spring constant values that can be obtained for these controllable parameters. Interestingly, it appears that the peak at a fiber separation of 100 μm gives rise to the largest spring constant values for both balanced and unbalanced powers. We estimate that this ideal 100 μm separation for achieving the highest spring constant values is due to the near field beam properties, as well as the characteristic beam divergence angle for our incident wavelength (λ = 980 nm) at a certain distance from the fiber end. Thus, it is presumed the curve profile shapes and peak spring constant values are characteristic of incident wavelength. This finding indicates that our system can be tuned to achieve desired spring constant values by careful control of power settings and fiber separations.

Fig. 6. Theoretical plots illustrating spring constant as a function of fiber separation for various power settings for left and right outputs (P_1 and P_2, respectively) illustrated by different curves. Curves were plotted according to the spring constant expression (Eqn.1). **(a)** Three curves demonstrate a broad range of fiber separations for balanced output powers ($P_1 \approx P_2$). **(b)** Six curves demonstrate a broad range of fiber separations for both balanced and unbalanced output powers.

Figure Legend:
o : P_1 = 0.049 W and P_2 = 0.045 W (Balanced Powers); x : P_1 = 0.044 W and P_2 = 0.041 W (Balanced Powers); ∇ : P_1 = 0.024 W and P_2 = 0.022 W (Balanced Powers); * : P_1 = 0.069 W and P_2 = 0.045 W (Unbalanced Powers); Δ : P_1 = 0.069 W and P_2 = 0.041 W (Unbalanced Powers); + : P_1 = 0.044 W and P_2 = 0.022 W (Unbalanced Powers)

(a)

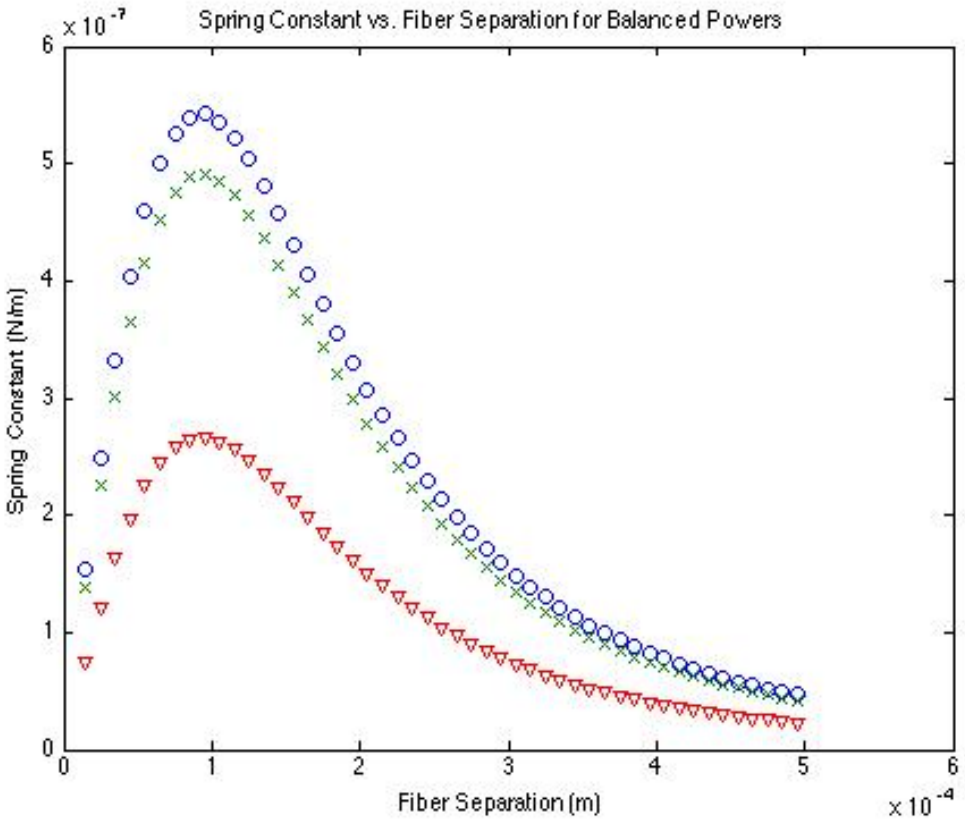

(b)

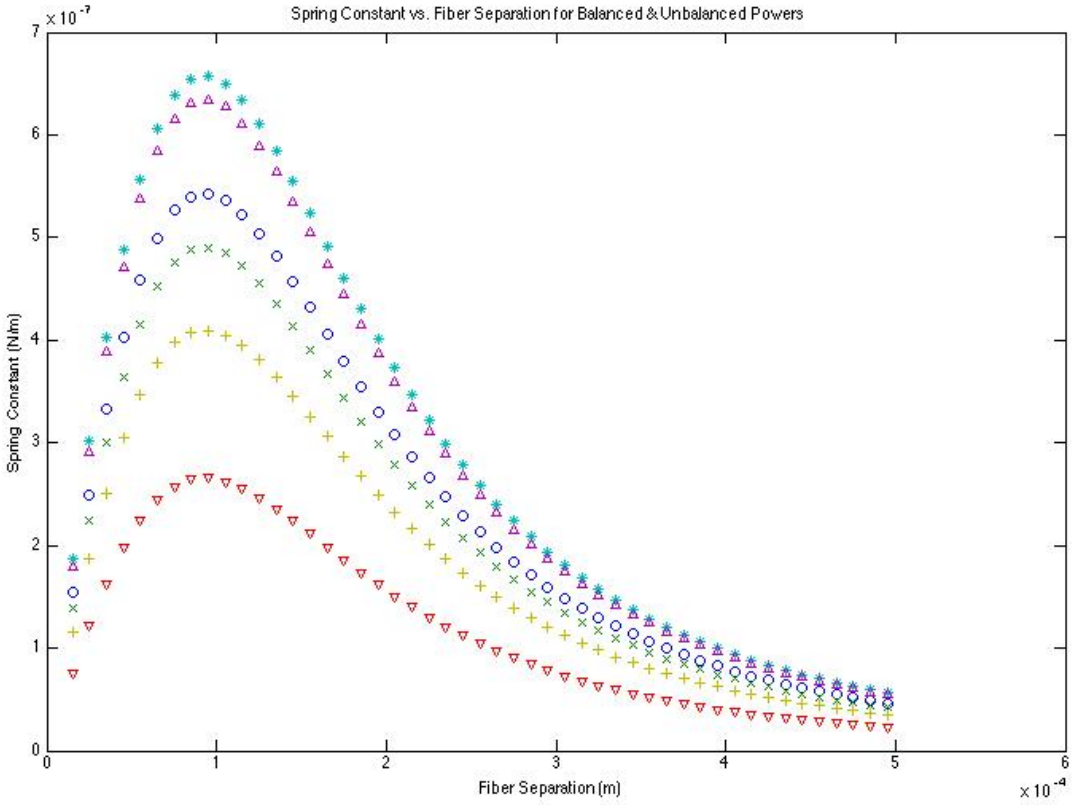

In order to further characterize our trapping system, we estimate the net scattering force acting on a trapped microsphere within a dual-beam fiber trap, as well as map the potential energy well present in the trapping region. Force quantities and potential energy values are dimensionless, and are solely meant to illustrate their relative profile shapes rather than define specific values. These mappings are based on trapping with balanced powers, laser wavelength λ = 980 nm, and a fiber separation of 100 μm. As illustrated in Fig. 7a, the net scattering force at 50 μm is zero for a microsphere in the center of trap. As expected, the scattering force profile reflects Gaussian behavior, such that the intensity drops off exponentially with increased distance from the fiber end. Also note the fiber separation region at ~40 μm to 60 μm: here the system forces behave in a linear fashion for a given microsphere displacement from the trapping

center. Fig. 7b depicts the potential energy profile due to the scattering forces acting on a trapped microsphere for a balanced power scenario. The zero potential energy location is chosen to be the end face of one of the fibers. The minimum potential energy is located at 50 μm from the fiber end, corresponding to a stable trap in the center of the trapping region.

Fig. 7. (a) Theoretical plot of net scattering force as a function of distance from fiber end for a microsphere trapped in a dual-beam fiber trap. **(b)** Theoretical plot depicting the potential energy well for our dual-beam trap.

(a)

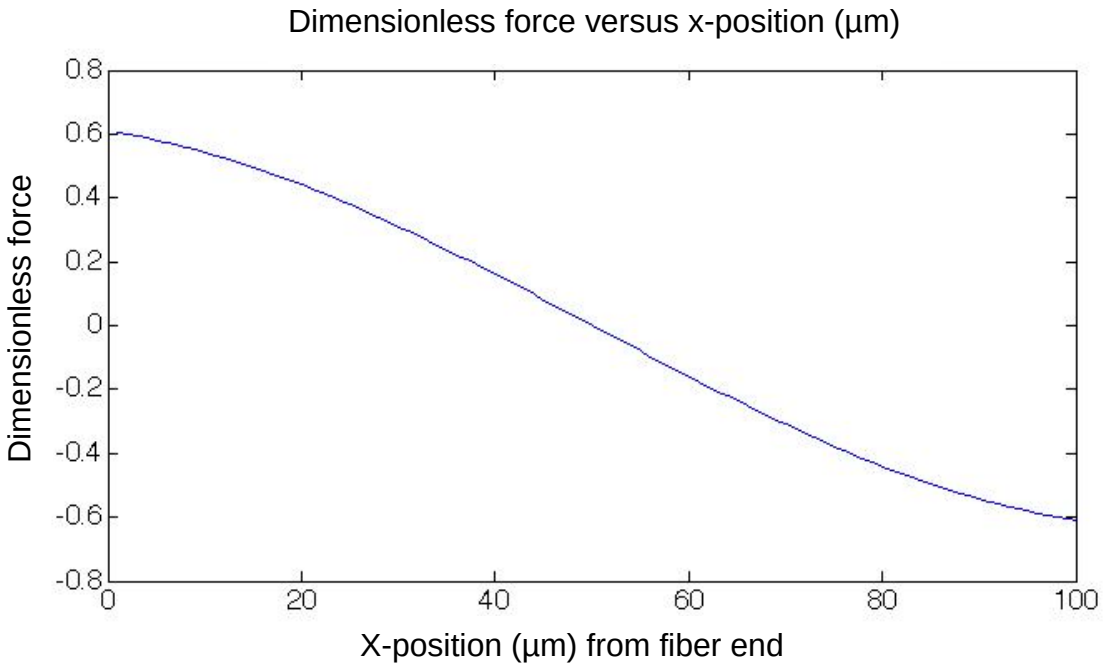

(b)

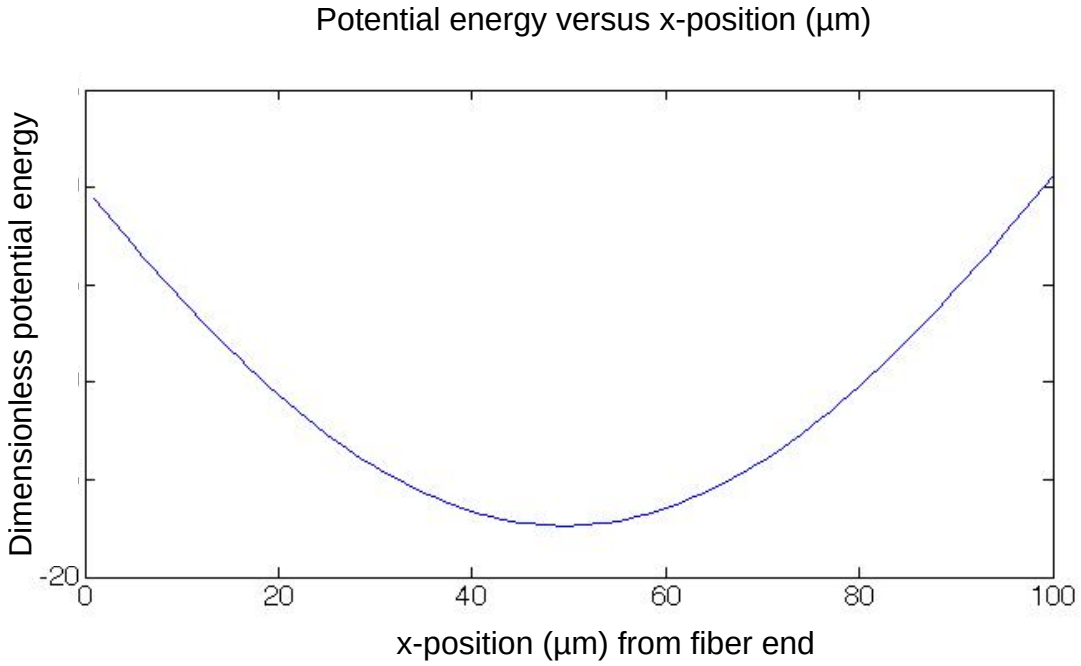

Methods

Basic scheme

Our dual-beam fiber configurations have an incident wavelengths of λ = 980 nm and do not use external focusing lenses or mirrors. The configurations consist of two overlapping diverging beams with Gaussian intensity profiles in the trapping region [Constable 1993]. Although we will need to perform cell viability tests for our trapping set-up, we anticipate our dual-beam trap offers the benefit of reduced intensity in the trapping region due to the lower power density in the trapping region [Grover 2001].

The optical trapping configuration uses simple, non-consumable materials and communication-grade diode lasers. Here we report on our initial trapping design with XYZ translational optical stages and highlight the calibrations we perform on the system. Our latest trap-on-a-chip approach affords a unique method to optically align counter-propagating optical fibers. As an extension of our fiber-pair configuration, we have exploited 2- and 4-fiber arrays of aligned traps.

In this experimental investigation, we design a trapping scheme in which two opposing beams of λ = 980 nm propagate through aligned single-mode optical fibers. Geometric optics is suitable to model the ray dynamics of our system, such that the two laser beams are treated as an infinite number of optical rays in the direction of beam propagation. The dual-beam optical trapping field is modeled as two opposing Gaussian beams such that light from each fiber diverges at angle θ with increased distance from the beam waist, ω_o, where Z is the distance from the fiber end [Hecht 2002]. For our trapping set-up, the highest beam intensity is situated at the beam waist, the point at which the beam emerges from the fiber. [Hecht 2002]. As illustrated in Fig. 8, the Rayleigh range, Z_R, is defined as the distance along a propagating Gaussian beam

where the radius increases by a factor of $\sqrt{2}$ and the beam cross-sectional area is doubled [Hecht 2002].

Fig. 8. Schematic illustrating the parameters of a Gaussian beam emerging from an optical fiber. The beam exits from the single-mode fiber with wavelength λ propagating along the z-axis. The beam diverges with angle θ along the beam path. Transverse to the direction of propagation the light has a Gaussian intensity gradient profile such that the highest intensity I(r) occurs at the beam waist, ω_o, the initial point at which the beam emerges from the fibers.

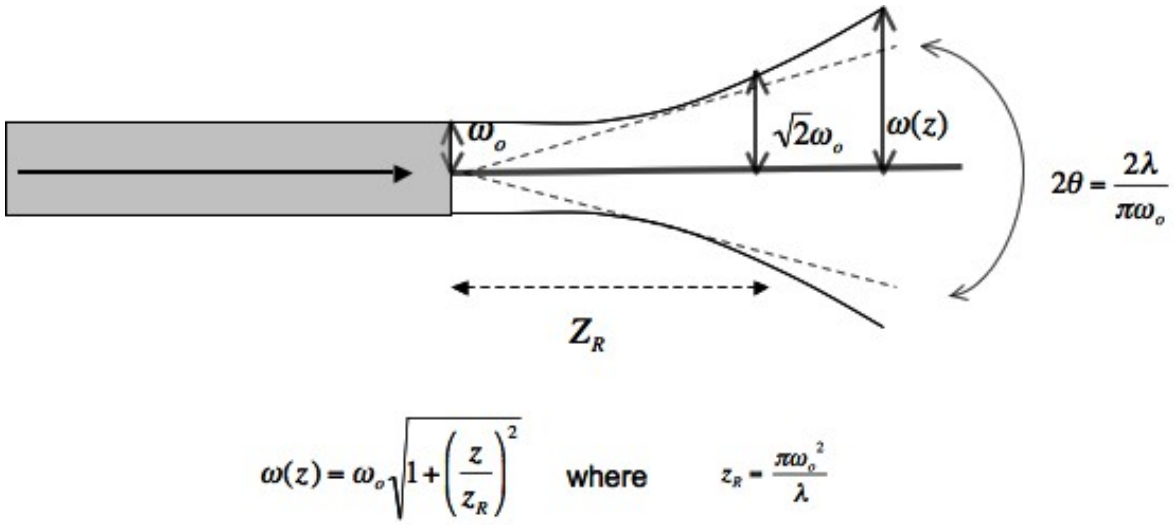

In our trapping experiment, a Gaussian beam of 980 nm wavelength light propagates through single-mode optical fibers with beam waist radius, ω_o, of 5 micrometers and numerical aperture of 0.14, as per manufacturing specifications (Fiber Instrument Sales, Oriskany, NY). We estimate the largest trapping area to be 226 μm^2 for a fiber separation of ~160 μm.

Our basic dual-beam optical trap set-up involves two opposing fiber-coupled beams that are manually aligned with respect with one another. The center region between two separated fibers (~20 μm to ~200 μm) provides a trapping space for micron-sized particles. An optically trapped particle in a Gaussian beam behaves like a particle in a harmonic potential well [Kawano 2008]. Single or multiple particles can be optically trapped, and within the trapping field they rearrange to sit in low potential energy wells [Singer 2003]. In the longitudinal (z) direction, the minimum in potential energy corresponds to the minima of beam intensity as a function of z [Singer 2003, Kawano 2008]. In the transverse (x-y) direction, the minimum in potential energy is the result of induced electrostatic dipole moments of a particle due to a light intensity gradient [Ashkin 1983].

The trap includes two fiber pigtailed continuous-wave diode lasers (λ = 980 nm, Agere Systems SL980, Allentown, PA) (Fig. 9). Optical trapping of polystyrene microspheres is conducted using light emerging from two bare single-mode optical fibers (SMF28E+, Fiber Instrument Sales, Oriskany, NY), with each fiber held in place by a fiber clamp on an XYZ translation stage (NanoMax TS 3-Axis Flexure, Thorlabs, Newton, NJ).

Fig. 9. Schematic and picture of a dual-beam trapping set up. **(a)** Microsphere trapping is conducted with two bare, counter-propagating single-mode fibers that are aligned with two 3-axis translation stages. The bare fibers are separately pig-tailed to two 980 nm diode lasers. Microspheres are trapped in water solution on a microscope slide. Real-time trapping is viewed from a microscope/CCD camera system and images are captured on the data acquisition computer. **(b)** Picture of trapping design equipped with XYZ stages: 3-axis translational stage (left) and multi-axis translational stage with angle alignment capabilities (right). The trapping region is indicated by the arrow.

(a)

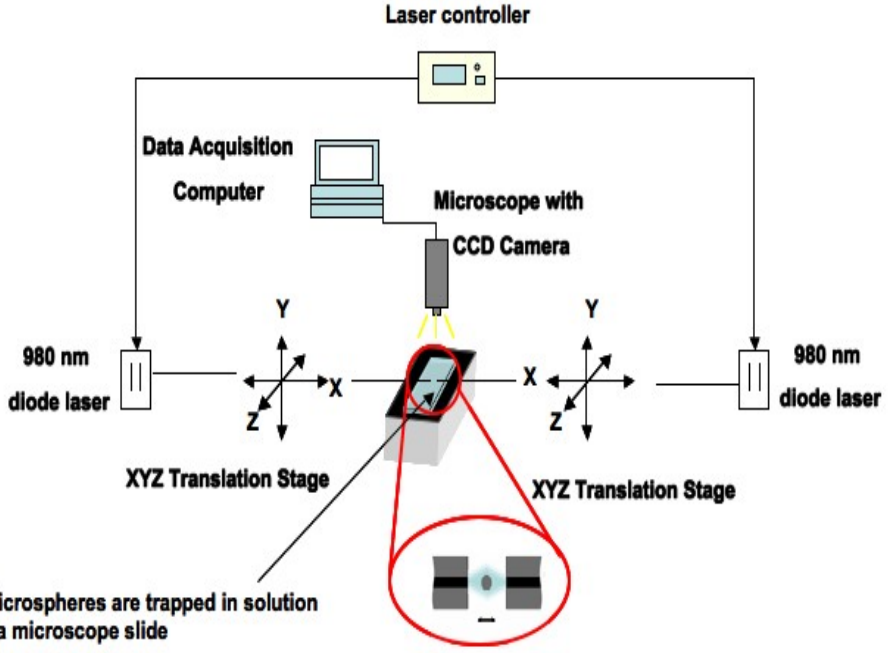

(b)

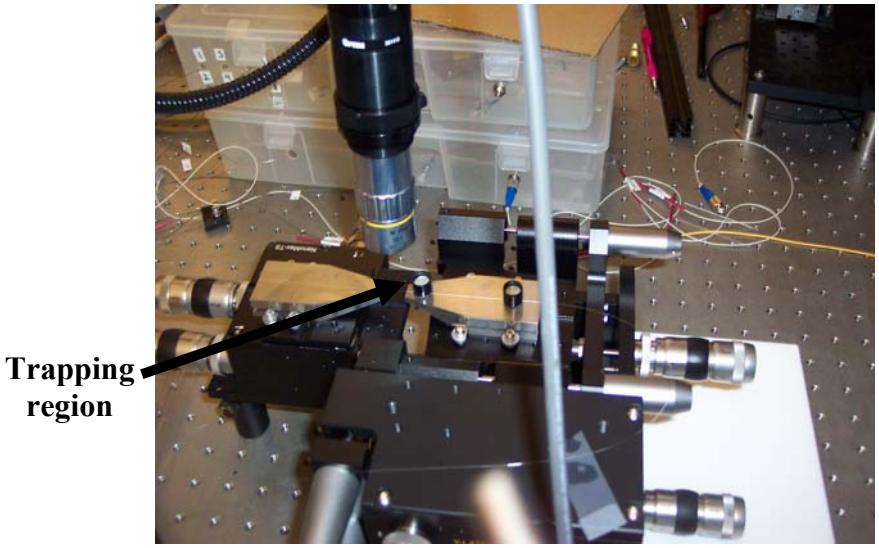

The fibers are manually positioned on the translation stages to maximize power coupling into one another as measured on an optical power meter (Orion-PD-ROHS, Ophir-Spiricon Inc., Logan, UT). This power coupling approach is taken to assure that the trapping beams are exactly counter-propagating (Fig. 10). Variations of misalignments can occur: translational displacements as well as rotational misalignments in which the fiber faces are skewed from one another. Excellent alignment (~2 ± 1 μm) is extremely critical in order to achieve steadily trapped microspheres. Translational misalignments (to be discussed in detail later) can induce oscillatory particle motion within the trapping region. Increasing the power outputs in both directions and adjusting the fiber separations also enhanced particle stability in the trap.

Particles

Plain polystyrene microspheres (10.2% (% w/v) suspension in DI water + 0.1% SDS, Bangs Laboratories, Inc., Fishers, IN and Corpuscular, Inc., Cold Spring, NY) of diameters 6 μm ± 0.37 μm and 10 μm are trapped in water solution (~0.005 g/mL, 0.5% w/v bead solution) on a small microscope slide placed under the aligned fibers. Fiber separations for trapping ranged from approximately 50 μm to 250 μm. Trapping powers range from the minimum of ~4-7 mW to a maximum of ~180 mW from each laser. The refractive index of the spheres is equivalent to 1.59, and is assumed to remain constant throughout the duration of the project. Particle concentration solutions utilized were 0.5 % w/v and 5% w/v. Through trial-and-error basis, the lower concentration of 0.5% microspheres freely floating in solution provided an ideal amount of spheres per volume of solution for single-sphere trapping studies. We find that higher microsphere concentrations increase the probability of multiple spheres falling into the trapping region, inducing uncertainty into damped motion calculations. Thus, at lower solution

concentrations single microspheres are trapped. Microsphere masses are calculated to be: 1.13×10^{-10} g (6μm spheres) and 5.24×10^{-10} g (10μm spheres).

Alignment procedure

To increase efficiency of the fiber alignment process, we used optical couplers (AC Photonics, Inc., Santa Clara, CA) with 50% coupling ratio spliced into the system. As shown in Fig. 10, the transmitted power from one fiber to the other can be maximized by monitoring the power on port "b" of each coupler while continuing to adjust alignment of the translation stage. This alignment method also showed to be beneficial in steadying the motion of a trapped microsphere.

Fig. 10. Basic fiber alignment technique via maximizing optical coupling. Laser light from Laser 2 is coupled into Fiber 1 (or vice versa) and power output is maximized to assure superb fiber alignment.

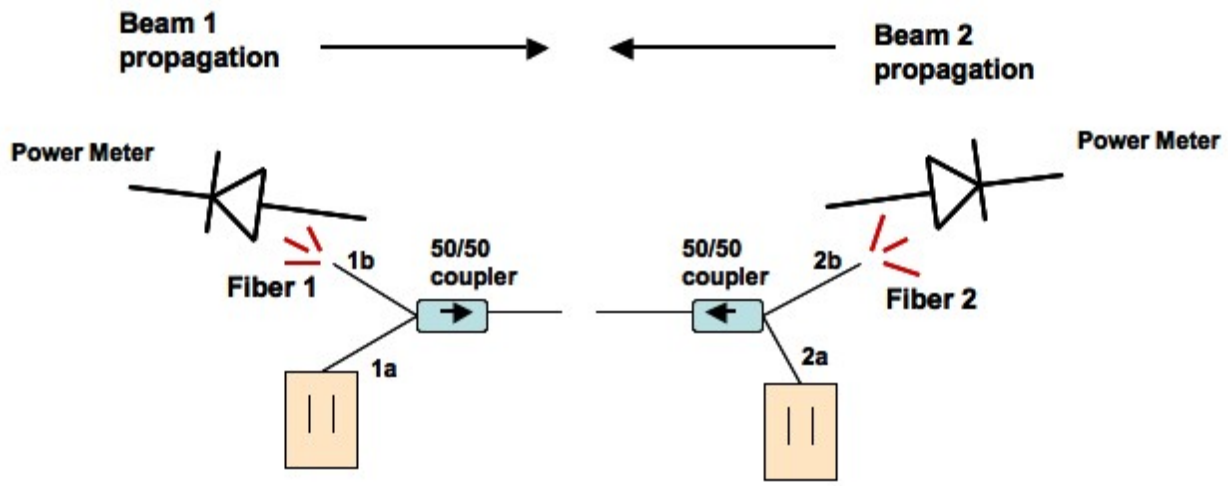

One other source of error is the uncertainty associated with misaligned fibers, causing trapped spheres to be unstably trapped. As discussed earlier, manually aligning fibers with the XYZ translational is quite tedious, taking as long as a few hours to align. Power output could

then be measured from the back end of one of the fibers to maximize coupling. Excellent alignment (± 1 μm) is required. Poor alignment causes the trapping potential energy surface to be misshapen. Rather than containing a single, well-formed concave potential well, misaligned fibers transform the depth of the well, causing it to become more shallow, or even cause two small potential wells to form. Effects of misaligned fibers can be seen in Fig. 11, when the trapped sphere sinusoidally oscillates within the trap. Less subtle fiber alignments sometimes cause two or three spheres to rotate and switch positions with one another sporadically, coming in an out of focus with respect to the microscope. These spheres appear to be held weakly within the trap. It is often possible to finely tune alignment while microspheres are still held in the trap; tweaking fiber alignment can drastically improve the steadiness of a trapped sphere. A representation of trapped particle motion when the optical fibers are transversely misaligned is shown in Fig. 11. As can be seen, the particle undergoes a rhythmic sinusoidal motion within the trap.

Fig. 11. Example of microsphere (d = 10 μm) motion in trap when fibers are slightly misaligned in two directions.

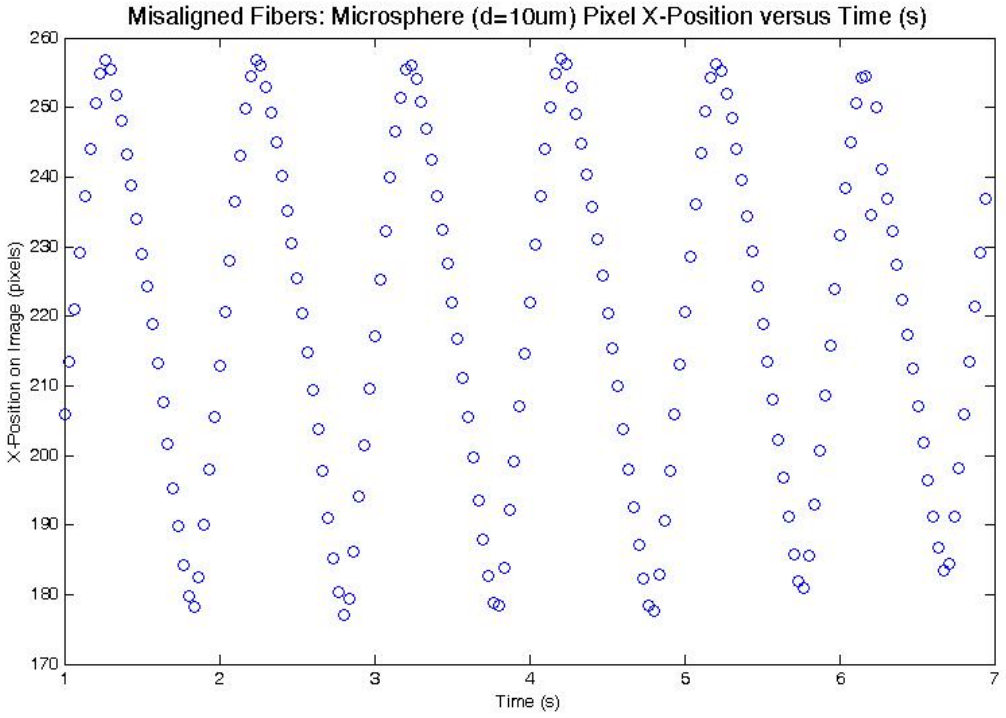

Experiment control and video acquisition

Trapped stationary and moving particles are imaged via a microscope (Thales Optem, Inc., model: Zoom 125, Fairport, NY) with 10x/0.28 N.A. and 5x/0.14 N.A. objectives (Mitutoyo). Videos are captured at 30 frames per second from a digital color CCD camera (Industrial Vision Source, model: CCAM Series, Farmers Branch, TX) connected to the microscope. Images and videos were viewed via the video capturing software (Hauppage WinTV-HVR 950, Hauppauge, NY).

During the trapping process, it can be difficult to determine whether one or two microspheres are trapped because the trapped spheres scatter the 980 nm incident laser light which appear as intense blue scattered light when viewed with the CCD microscope camera. To

circumvent this problem, an optical filter (type: SPF 900, CVI Melles Griot, Albuquerque) is placed over the microscope lens to filter out the scattered light. Using this method we can verify that only one microsphere is in the trap.

A suitable frequency of power modulation from one laser channel was determined to be 0.17 Hz. Power modulation amplitude is an input parameter that repeatedly changes the initial power from the base power. To verify that the laser powers were being modulated in a periodic square-wave fashion, we observed the power modulation on an oscilloscope (LeCroy WaveSurfer®, model: Xs Series, Chestnut Ridge, NY) with a fast photodiode (Electro-Optics Technology, Inc., ET-2030 Silicon PIN Detector, Traverse City, MI). Oscilloscope traces confirm that the diode lasers exhibit the expected minimal amount of background noise. We also confirm that both diode laser powers are being modulated instantaneously, as seen by the vertical edges of the pulse trains. This verifies that when a trapped microsphere is displaced from its equilibrium position via a sudden change in laser power, the microsphere exponential trajectory is truly a response to the power change. The fastest frequency that could be utilized in our LabVIEW (version 8.2, National Instruments, Austin, TX) rectangular modulation program was 4 KHz. When the frequency setting was set at a faster rate, the laser modular controller does not respond properly.

The effectiveness of the program strongly depends on the illumination of the trapped microsphere, particle focus on the camera, particle size, and most importantly, the velocity of the moving sphere. One limitation of the system is the relatively slow frame rate (30 fps) of the image acquisition system that restricts the number of positions that can be tracked per time. Depending on particle size and amount of sphere displacement, the shortest time constant (of the

exponential sphere trajectories is estimated to be approximately 0.13s to 0.17s that can be accurately tracked with our CCD camera system.

Video clips in mpg format (30 sec. to 60 sec. long) of microsphere oscillations within the trap are recorded. The MATLAB particle tracker program is set to analyze 30-second intervals of particle motion. The particle tracking program, written by Blair and Dufresne [2008], allows the position of one microsphere to be tracked as a function of time. The particle tracking program can track one trapped microsphere; it is presumed that having multiple trapped microspheres will introduce uncertainty to the spring constant calculations. Microsphere positions as a function of time are extracted from videos using the particle tracking MATLAB program and utilizing a digital CCD camera system recording at 30 frames/second. Results indicate that particle tracking is achievable with sub-pixel resolution (1 pixel $\approx$ 1 μm). In order to explore the underlying trapping mechanics, including spring constants and restoring forces, the microsphere motion is fitted to an exponential function to reflect an overdamped system.

The MATLAB particle tracking program is capable of reading .mpg format video clips. It analyzes the movie as a series of pictures via functions that track particle position (in pixels) versus time in seconds. A summary of the MATLAB particle tracking functions is described in Fig. 12. The main mpg tracking program calls eight other MATLAB files, and each file has a different role in the process particle tracking. The program is comprised of carefully selected image processing parameter filters that track the particles in real time, calculating the bright centroid (cntrd.m) of the particle every time a frame is registered by the camera. The program turns the movie into an array that first looks at the negative of each image (Fig. 13). Subsequently, it looks at the blue part of the image (the trapped microsphere), and then makes it a positive image again. The bandpass filter program (bpass.m) suppresses background noise and

image variations in order to locate the particle of interest. Then the program scans for a peak (pkfnd.m) for an object about 11 pixels wide, until the centroid (cntrd.m) of the microsphere is found. The results are saved as output data arrays. Image processing parameters are easily modified to optimize the tracking process.

Fig. 12. Summary of MATLAB particle tracking process from an uploaded .mpg format video clip. The program employs a series of algorithms to locate particle position as a function of time for the entire length of the video.

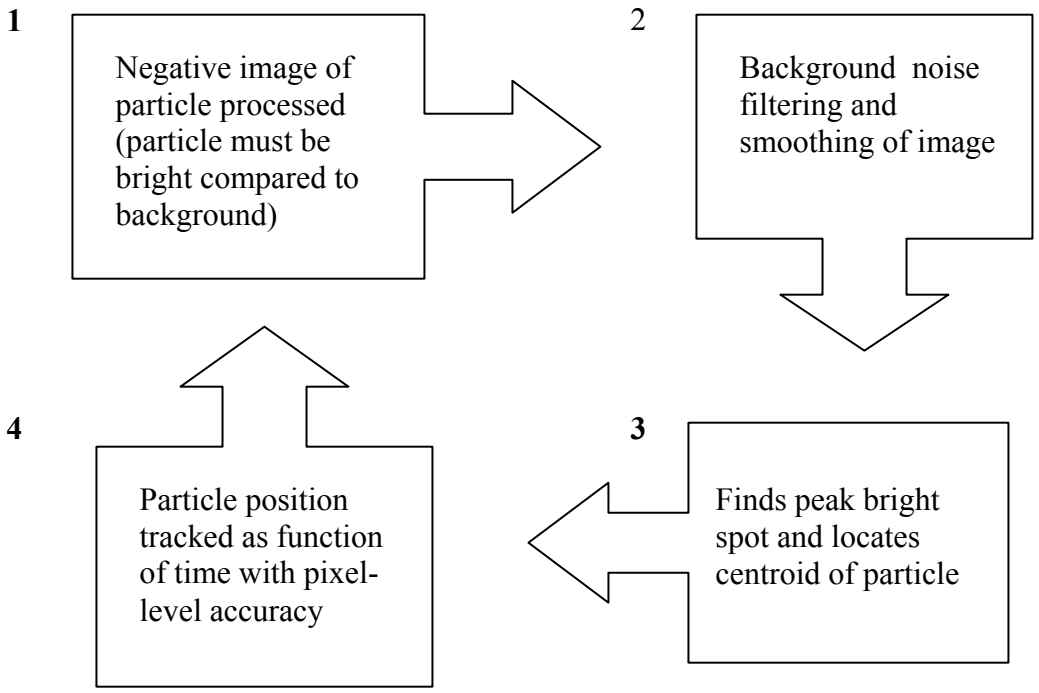

Fig. 13. Images of optically trapped 6- and 10 µm spheres in water. Fibers aligned via XYZ translation stage design. **(a)** Video snapshot of 6 µm polystyrene sphere trapped with ~47 mW power output. Fiber separation ~163 µm. **(b)** Respective negative image of 6 µm sphere from MATLAB particle tracker program after video upload into the tracker program. MATLAB program converts image matrices into pixel format for tracking process. **(c)** Video snapshot of 10 µm polystyrene sphere trapped with ~47 mW power output. Fiber separation ~104 µm. **(d)** Respective negative image of 10 µm from MATLAB particle tracker program after video upload into the tracker program. MATLAB program converts the image matrices into pixel format for tracking processes.

(a)

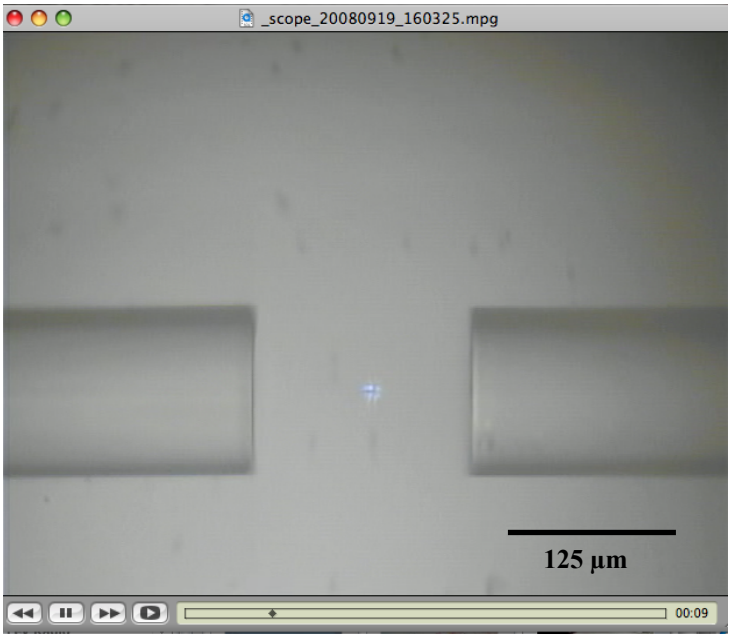

(b)

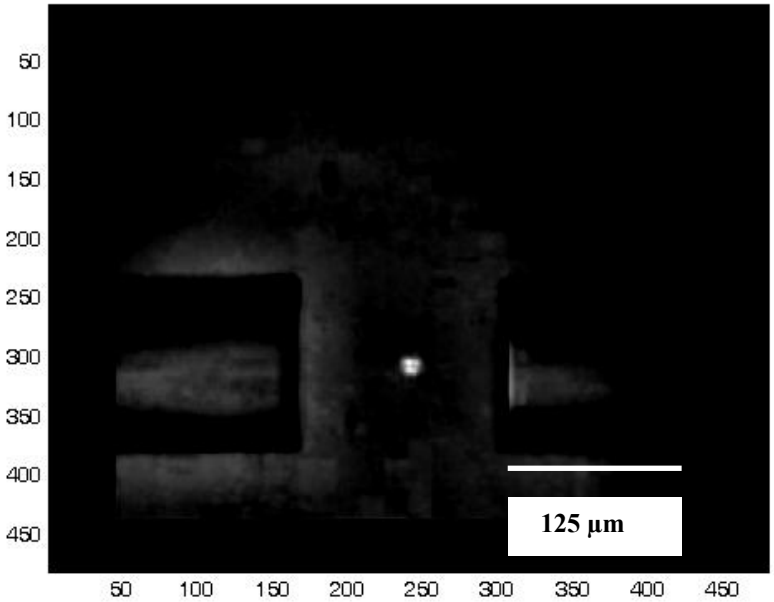

(c)

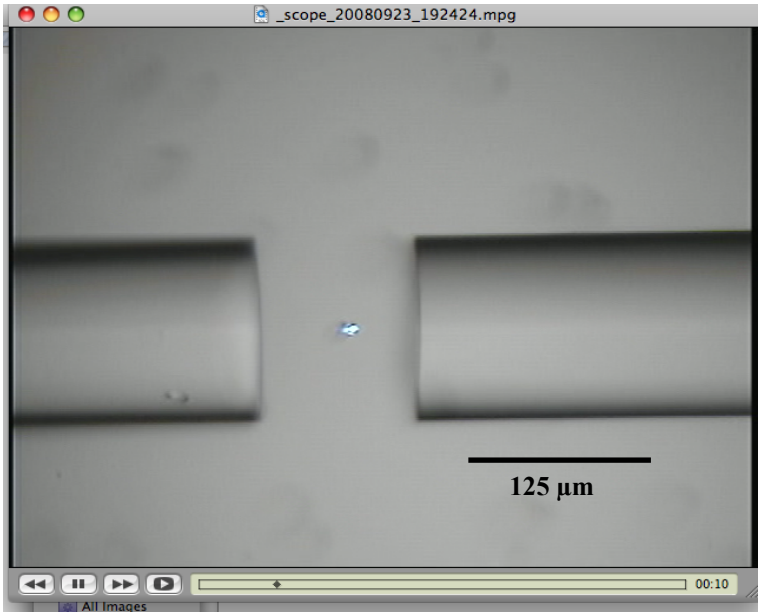

(d)

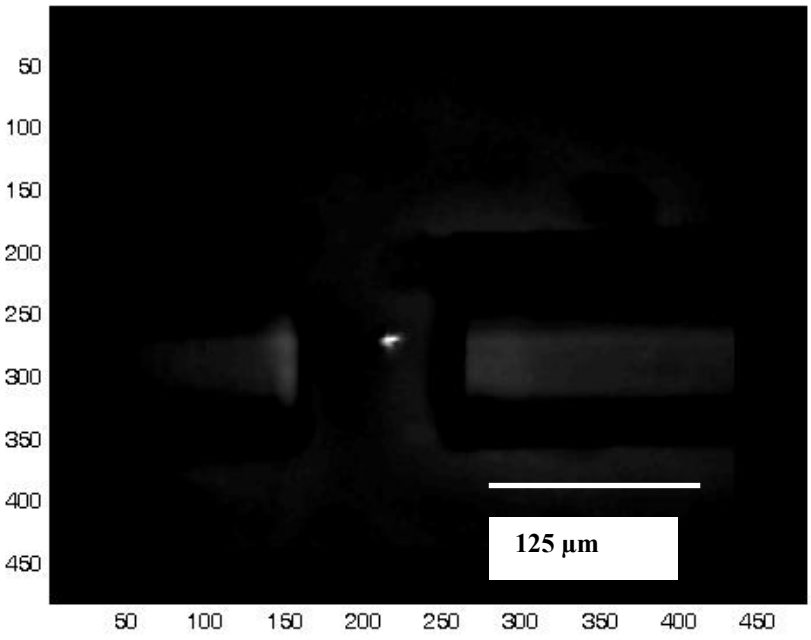

Y-Position (Pixels)

X-Position (Pixels)

In order to assess the motion noise from a single trapped microsphere (with both lasers set to about the same power, $P_1 \approx P_2$), we tracked the motion of the microsphere in trapped "equilibrium state." Fig. 14 and Fig. 15 illustrate microsphere position (in two directions) as a function of time.

Fig. 14. MATLAB particle tracking program plot of trapped microsphere (d = 6 μm) at constant laser power (before laser power modulation). Laser 1= 49 mW and Laser 2 = 45 mW, and fiber separation = 125 μm. These figures demonstrate the natural noise of the system. **(a)** Plot of X-position (pixels) as a function of time. **(b)** Plot of Y-Position (pixels) as a function of time.

(a)

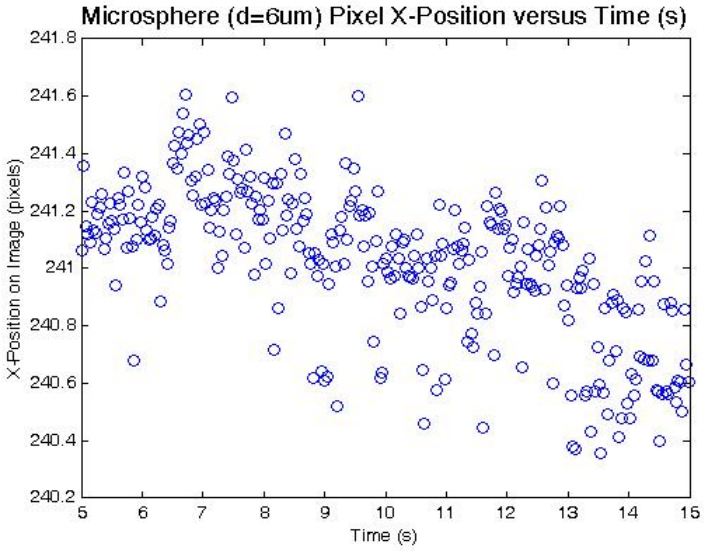

(b)

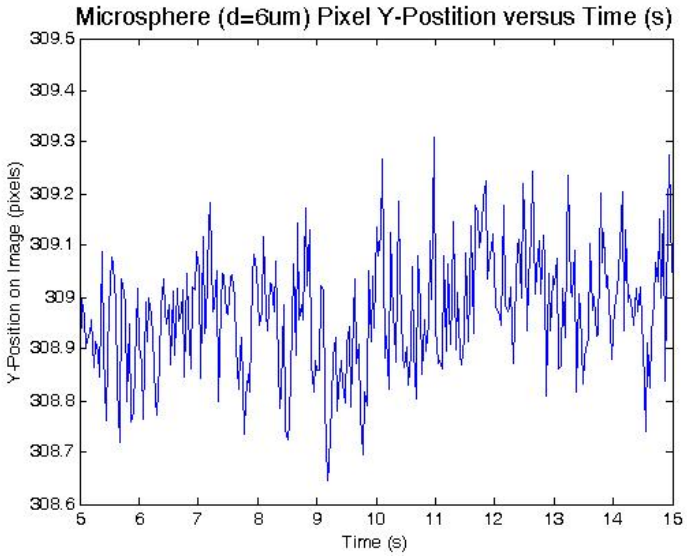

Fig. 15. MATLAB particle tracking program plot of trapped microsphere (d = 10 μm) at constant laser power (before laser power modulation). Parameters utilized: P_1: 49 mW and P_2: 45 mW, and fiber separation = 77 μm. The following plots demonstrate the natural noise of a trapped microsphere before modulation. **(a)** Plot of X-position (pixels) as a function of time. **(b)** Plot of Y-Position (pixels) as a function of time.

(a)

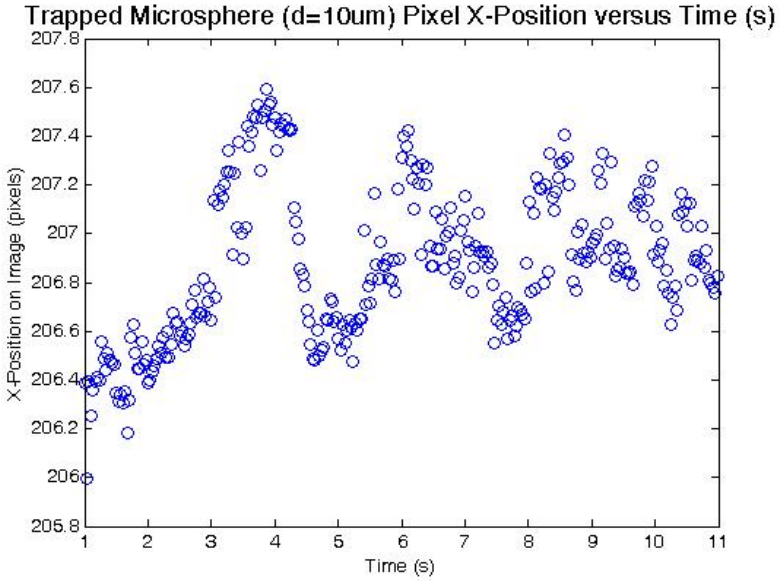

(b)

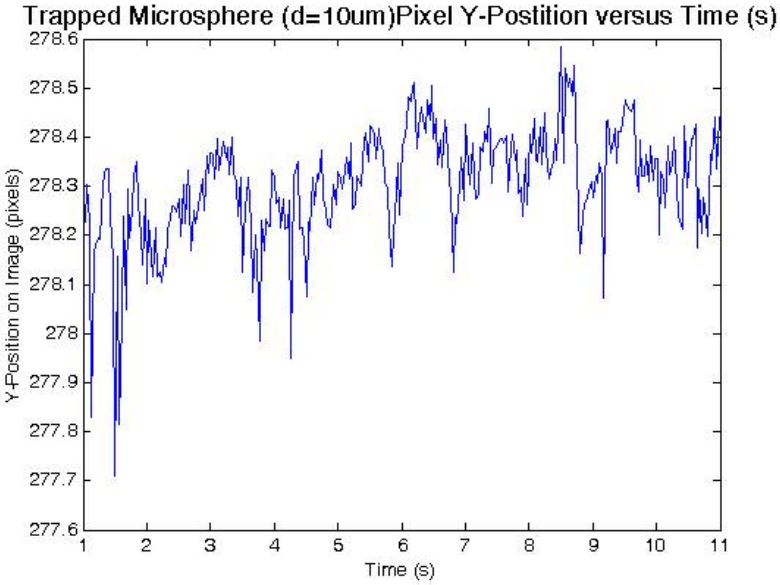

Obtaining trap parameters from tracking data

We measure κ after tracking the particle's x-position as a function time with the CCD camera and video/frame grabber software. Upon analyzing microsphere motion in the trap using our MATLAB particle tracking program, the data of was imported into IGOR Pro v. 6.0 (Lake Oswego, OR), for data analysis.

The spring constant κ (N/m) is determined for a strongly overdamped system for a particle moving through water. Particle position versus time exponential motion curves are fitted to: $\varepsilon = c_1 e^{(-\kappa\tau/6\pi\mu R)} + c_2$ and κ is given by the following formula: $\kappa = \frac{6\pi\mu R}{\tau}$ where μ is the viscosity of water (at 25ºC) = 0.89x10^{-3} Pa·s; R = microsphere radius (m); τ = time constant (s) as determined from IGOR PRO exponential curve fitting. Note that constants c_1 and c_2 are not needed for the spring constant calculations.

Theoretical spring constants (κ) are computed according to Eqn. 1 for incident light upon a dielectric sphere of a given area being trapped with two counter-propagating beams with constant intensity and phase values:

$$\kappa = 16\pi^2 aS\left[\frac{P_1 Q_{pr,1}\omega_{0,1}{}^2}{\lambda_1{}^2(S^2+4d_1{}^2)^2} + \frac{P_2 Q_{pr,2}\omega_{0,2}{}^2}{\lambda_2{}^2(S^2+4d_2{}^2)^2}\right] \qquad \textbf{(Eqn. 1)}$$

where $a = 2R^2/c$ (the incident geometrical cross-sectional area of the sphere), and R = sphere radius (R = 3 μm and R = 5 μm); c = velocity of light in a vacuum; P = incident power; $d^{-1} = \lambda/(\pi\omega_0{}^2)$, where λ= incident laser wavelength (980 nm) and ω_o = Gaussian beam waist (5 μm); S = fiber separation (typical range 50 μm to 250 μm); Q_{pr} = radiation pressure coefficient which was calculated from C. Mätzler's "MATLAB Functions for Mie Scattering and

Absorption" program [2002]. We calculate the Q_{pr} values for our microspheres to be: Q_{pr} = 0.2968 (for R = 3 μm) and Q_{pr} = 0.2013 (for R = 5 μm). Fiber separations are measured using scaling capabilities on ImageJ, a public domain image processing and analysis software [NIH.gov].

The total scattering force (F_s) for both fibers is also calculated from the following expression (Eqn. 2):

$$F_s = \frac{aP_1Q_{pr,1}/\omega_{0,1}^{\ 2}}{1+d_1^{-2}(S/2+z)^2} - \frac{aP_2Q_{pr,2}/\omega_{0,2}^{\ 2}}{1+d_2^{-2}(S/2-z)^2} \qquad \textbf{(Eqn. 2)}$$

where z is the distance from the center region between the fibers (i.e. z = 0 corresponds to the center point). It is expected that when both output powers are equal to each other the net scattering force is 0, since the opposing force vectors balance one another. All other parameters in the scattering force expression are previously defined above for the spring constant calculation.

Power modulation experiment procedure

We also evaluate the behavior of our trapped microspheres when one laser power is suddenly increased and then restored back to the original power. In response to the power change, the microsphere rapidly changes its x-direction position. The water provides a highly overdamped environment, causing the microsphere motion to exponentially decrease and approach zero velocity. We investigated the motions of the both sizes of spheres (d = 6 μm and d = 10 μm) moving through the water when power output from one laser is changed from 0.049 W to 0.069 W, while the other laser remains constant at 0.045 W (Fig. 16 and Fig. 17). All power modulations were performed at a 0.17 Hz frequency.

Fig. 16. MATLAB particle tracking program plots of displaced microsphere (d = 6 μm) position as a function of time. "Laser 1" power was systematically modulated from 49 mW to 69 mW using LabVIEW at 0.3Hz, while "Laser 2" remained constant at 45 mW. Fiber separation = 125 μm. **(a)** Plot of X-Position (pixels) as a function of time. **(b)** Plot of Y-Position (pixels) as a function of time.

(a)

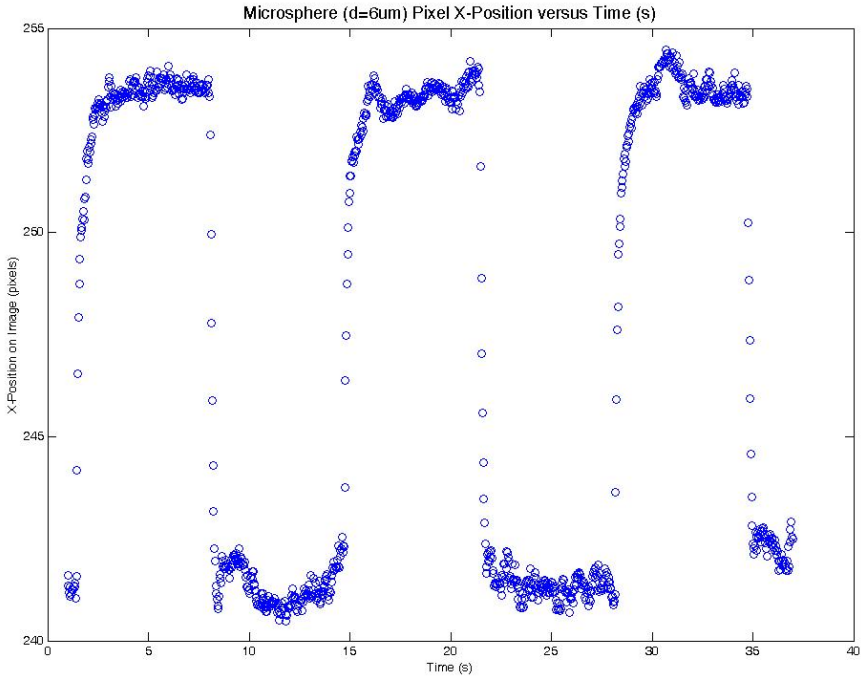

(b)

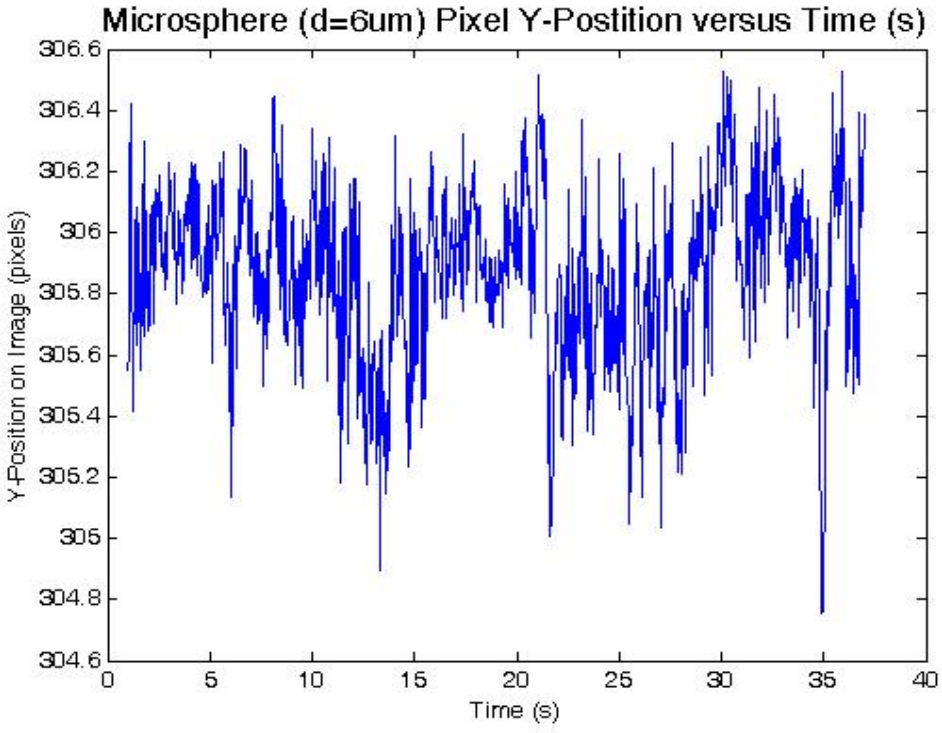

Fig. 17. MATLAB particle tracking program plots of displaced microsphere (d = 10 μm) position as a function of time. "Laser 1" power was systematically modulated from 49 mW to 69 mW using LabVIEW at 0.3Hz, while "Laser 2" remained constant at 45 mW. Fiber separation = 125 μm. **(a)** Plot of X-Position (pixels) as a function of time. **(b)** Plot of Y-Position (pixels) as a function of time.

(a)

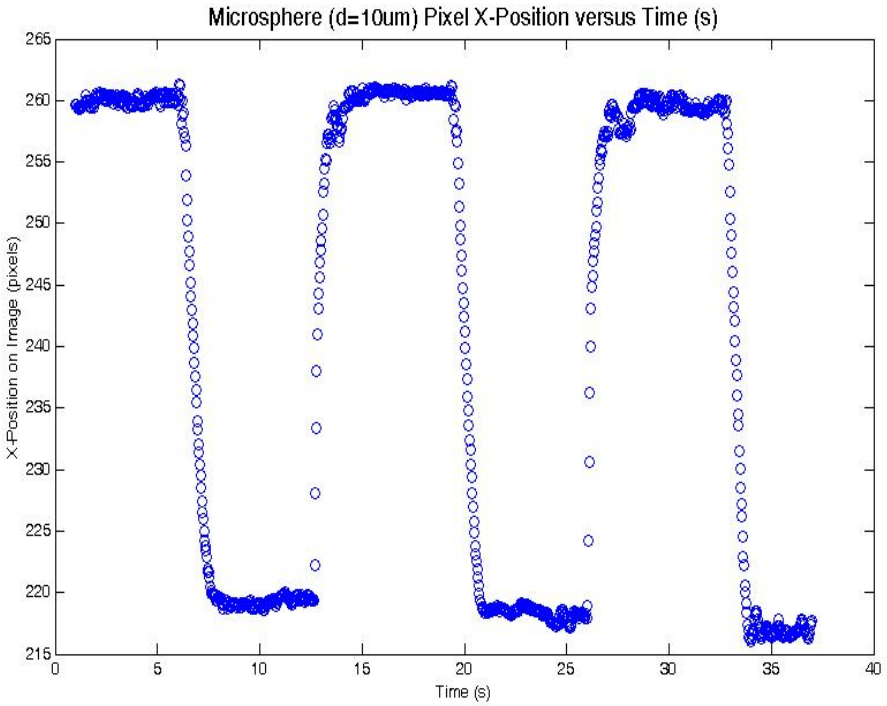

(b)

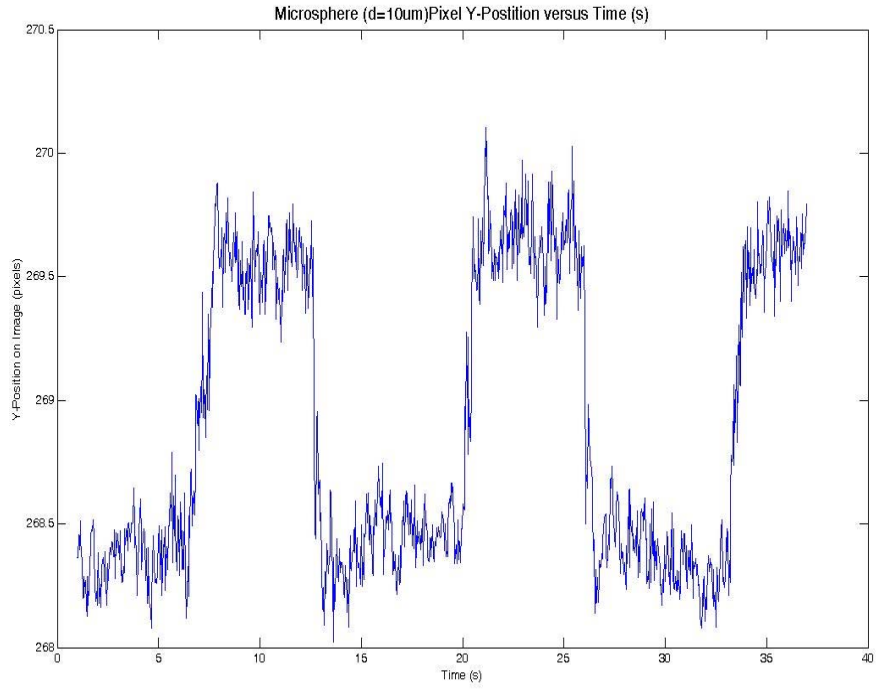

When we induce a sudden change in power from one laser, a trapped microsphere is displaced from the center of the trap. When analyzing our data we use the terms “increase exponential” and “decrease exponential” to refer to the motion of the trapped particles under two different conditions. Increase exponential curves refer to the microsphere falling into a trap formed when the total power is increased (one laser’s power has increased while the other has stayed the same). Decrease curves relate to the microsphere falling into the trap when the total power is decreased (the two lasers have approximately the same power as each other). Since the total power is larger while all other parameters stay the same, the spring constants will be larger (i.e. “stiffer spring” characteristic). In contrast, the spring constants will likely be smaller (i.e. less stiff of a spring) when the total power is reduced.

Heat-Etching Fiber Wave Guides in Cast Acrylic Plexiglass Chips

We developed a procedure for creating fiber alignment channels that simplifies our initial trapping design and allows 1, 2, or 4 fiber pairs to be aligned within the channels. Uniform fiber alignment channels are burned into black cast acrylic “plexiglass” chips (McMaster-Carr, Robbinsville, NJ) using high-resistive nichrome wires (36 gauge, Jacobs Online, Moxee, WA) that are the same diameter as the optical fibers (~125μm). Heated wires are ~7.0 cm in length for constructing 1- and 2- channel etchings, and ~10.0 cm in length for 4- channel etchings. These wires are pulled tight across electrical leads from a power supply (BK Precision, model 1672 Triple Output, Yorba Linda, CA) (refer to Fig. 18). One plexiglass chip cut to be ~2x2” is placed under the wires and a dummy chip is placed on top of the wire(s) and bottom chip to be etched. Depending on the number of channels desired, the appropriate amount of electrical current is conducted through the wire(s) according to the tabulated recipe (Table 1). Hanging weights (370 g each) are attached to the heated wires and hung off the table next to the main heat-etching set-

up. These weights provide constant wire tension even when the wires endure heat-induced expansion due to the electrical current. Small alignment rods are placed under the wire(s) (and on top of the etching chip) to serve as "rollers" and aid in providing a smooth, flat profile for the heating wire(s).

Fig. 18. Equipment set-up for heating-etching cast acrylic chips. **(a)** Power supply with electrical leads held in place with screws. Tension weights that provide tension to the nichrome high-resistive wires are shown hanging off the table edge. **(b)** Close-up shot of nichrome wires strung across electrical leads. The wires are clamped tight around the right electrical lead and are free to expand through a propped open clamp.

(a)

(b)

Table 1. Parameters utilized for heat-etching channels in cast acrylic chips with nichrome heater wires.

Number of Channels	Current (A)	Approximate Wire Length (cm)	Heating Time (s)	Tension Weights
1	0.75	7.0	90	1 weight, 370 g
2	1.1	7.0	90	2 weights, 370 g each
4	2.1	10.5	90	2 weights, 370 g each

It is important to note that for the two-channel scheme, we are able to string two wires next to each other (without any space between them) fairly easily. However, stringing together four wires, either right next to one another or evenly spaced, is very difficult with our current design. To remedy this issue, two small metric screws with thread separation of ~457 μm, are glued to very small plexiglass chips and placed under the heating wires to act as a bridging mechanism that keeps the wires straight, tight, and evenly spaced.

Once the fiber channels on the chip are heat-etched, we use a technique that keeps the optical fibers (single mode) in place and in their individual channels. The final chip arrangement provides a method to add a gentle downward bending tension so that the fibers are guided into the channels.

Small aluminum rods (Digi-Key Corp., Thief River Falls, MN) are super glued onto the chip for fiber alignment and positioning purposes. The two outer rods of the chip (refer to Fig. 19) are bonded directly onto the chip with super glue. The two center rods are raised up from the bottom of the chip. The back ends of these rods were glued onto a small microscope slide. This

design allows for an "over and under" approach to keeping the fibers in place. Subsequently, bare single-mode fibers are placed into the channels.

Fig. 19. Schematic and picture of the trapping chip layout. **(a)** Depiction illustrates 4 channel arrays on a cast acrylic "plexiglass" chip with bonded aluminum fiber alignment rods. Four fiber pairs are shown in their channels, with the alignment rods providing a gentle mechanical downward tension to the fibers. **(b)** Image of 2-channel heat-etched chip with two aligned fiber pairs for the 2x2 fiber array design.

(a) **(b)**

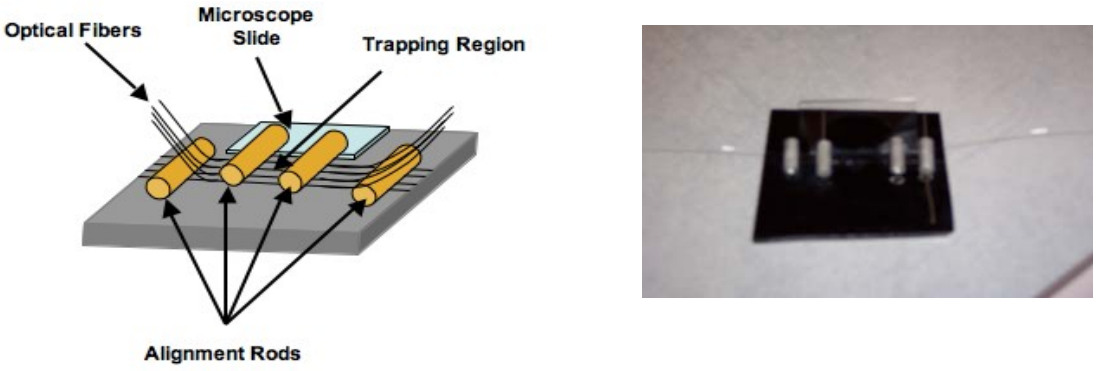

For the one- and two-fiber channel design, two bare fibers were utilized. For the four-fiber channel design, fiber ribbon cables (SMF, Fiber Optics for Sale Co., Milpitas, CA) is an easier option for manipulating and keeping the fibers aligned in the channels (see Fig. 20). Maximizing the output coupling from one of the ribbon cables into the other ribbon cable provides confirmation of good fiber alignment. Once positioned, the fibers are carefully superglued into place, while continuing to monitor the alignment by measuring the power transmitted through the trap.

Fig. 20. Schematic and picture of 4x4 fiber array trapping platform. **(a)** Schematic: Power from 980 nm laser is split seven ways through 50/50 couplers (50% coupling) and then spliced individually into 4-fiber ribbon cables. Bare fiber end extending from the fiber ribbon cables are inserted into the trapping platform scheme. **(b)** Picture of 4-channel heat-etched chip with two counter-propagating fiber cables, with each cable containing four fibers. This design was used for the 4x4 fiber array design.

(a)

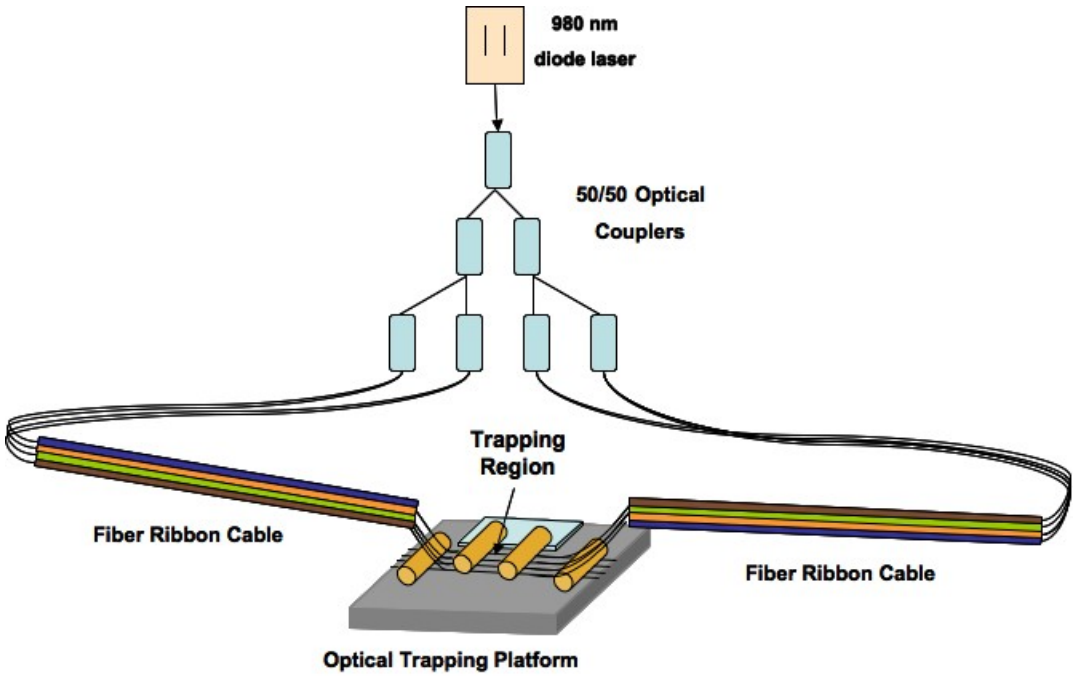

(b)

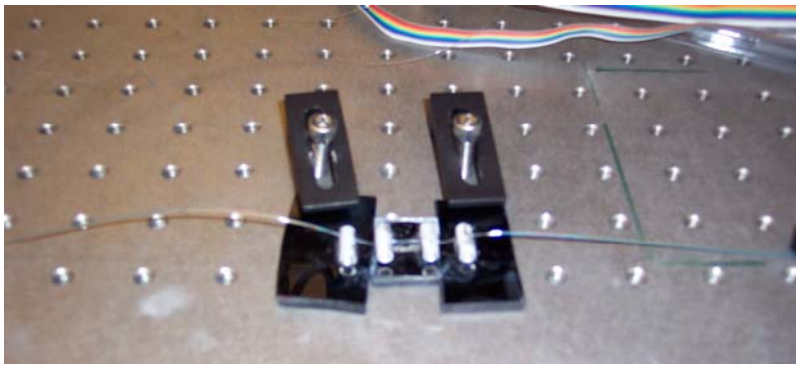

Results

Here we report on our initial trapping design with XYZ translational optical stages and highlight the calibrations we perform on the system. Using this setup we measure spring constants in the range from 100-500 nN/m by displacing a stably trapped microsphere (d = 6 μm and 10 μm) in water with a sudden change in power. By tracking particle motion as a function of time, we show particle motion exemplifies overdamped exponential motion in the water. We also report scattering force values of 9-60 pN.

Time constants for exponential decreases for the 6 μm spheres range from 0.117s to 0.478s for all experimental trials ($\kappa = 4.30\text{x}10^{-7}$ N/m and $\kappa = 1.05\text{x}10^{-7}$ N/m, respectively), whereas time constant for exponential increases range from 0.045 s to 0.252 s ($\kappa = 1.12\text{x}10^{-6}$ N/m and $\kappa = 2.00\text{x}10^{-7}$ N/m, respectively). Fiber separations ranging from 67.9 μm to 125 μm for 6 μm trapping assays are utilized. As expected, time constants and spring constants for the trapped 10 μm spheres are larger than those for 6 μm spheres for most of the trials conducted. Time constants for 10 μm range from 0.259 s to 0.511 s ($\kappa = 3.24\text{x}10^{-7}$ and $\kappa = 1.64\text{x}10^{-7}$ N/m, respectively). Time constants for exponential increases for the 10 μm spheres range from 0.126s to 0.258s ($\kappa = 6.66\text{x}10^{-7}$ N/m and $\kappa = 3.25\text{x}10^{-7}$ N/m, respectively). Fiber separation of ~77.0 μm is used for all 10 μm trapping experiments.

Example IGOR PRO curve fits are shown in Fig. 21 for the same assays performed in Fig. 16 for 6 μm- and Fig. 17 for 10 μm spheres. Respective experimental and theoretical spring constant values are shown in the tables below in Fig. 21. Scattering forces exerted onto a trapped microsphere from the left and right are calculated from Eqn. 2.

Fig. 21. Exponential curve fits of microsphere x-position motion through water due to a sudden change in laser power. **(a)** Exponential curves for 6 µm microsphere and **(b)** respective chart of calculations for each periodic increase and decrease. **(c)** Exponential curves for 10 µm microsphere and **(d)** respective chart of calculations for each periodic increase and decrease.

(a)

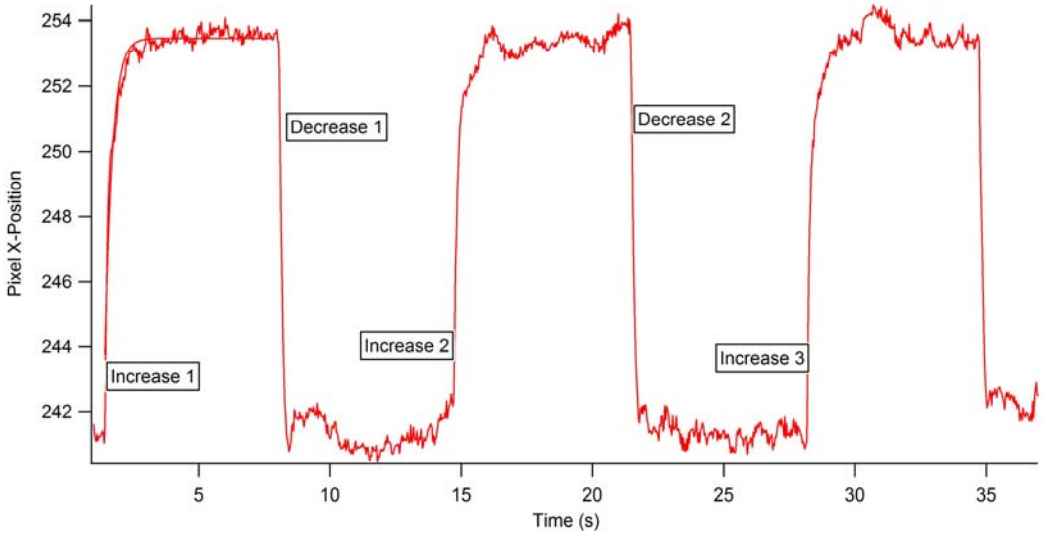

(b)

Exponential Curve	Time constant τ (s)	Spring Constant κ (N/m)	Theoretical Spring Constant κ (N/m)	Left Scattering Force (pN)	Right Scattering Force (pN)
Increase 1	0.252	2.00×10^{-7}	6.11×10^{-7}	25.6	23.6
Decrease 1	0.117	4.30×10^{-7}	5.04×10^{-7}	20.9	20.7
Increase 2	0.234	2.15×10^{-7}	6.11×10^{-7}	25.6	23.6
Decrease 2	0.121	4.16×10^{-7}	5.04×10^{-7}	20.9	20.7
Increase 3	0.225	2.24×10^{-7}	6.11×10^{-7}	25.6	23.6

(c)

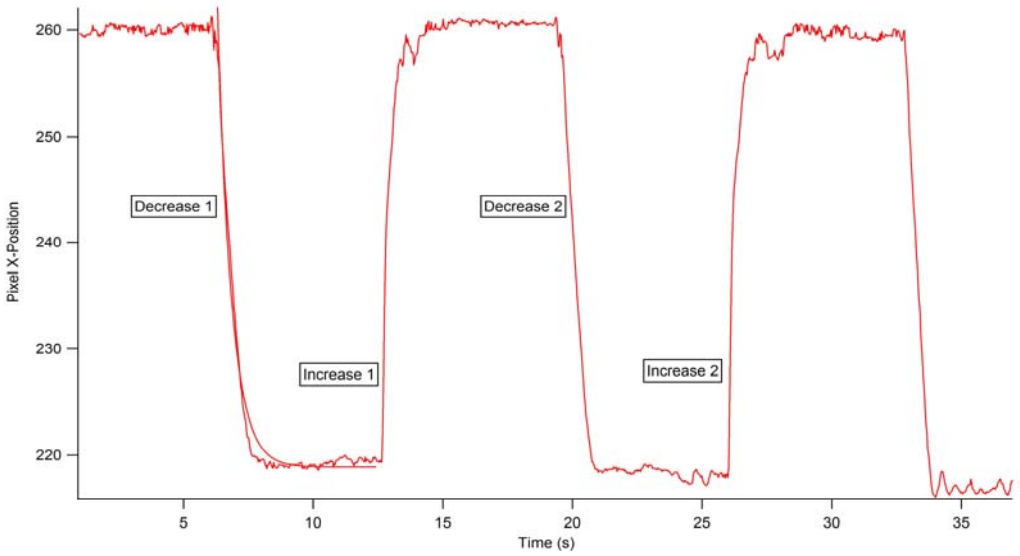

(d)

Exponential Curve	Time constant τ (s)	Spring Constant κ (N/m)	Theoretical Spring Constant κ (N/m)	Left Scattering Force (pN)	Right Scattering Force (pN)
Increase 1	0.236	3.55×10^{-7}	1.21×10^{-6}	49.1	60.4
Decrease 1	0.511	1.64×10^{-7}	9.98×10^{-7}	50.4	51.7
Increase 2	0.258	3.25×10^{-7}	1.21×10^{-6}	49.1	60.4
Decrease 2	0.49	1.71×10^{-7}	9.98×10^{-7}	50.4	51.7

Several experimental assays with the 10 μm spheres were performed with approximate fiber separations of 76 ± 2 μm. The average spring constant values for exponential decreases is 2.2×10^{-7} N/m (σ = 0.6 N/m) when powers are balanced: P_1 = 0.049 W and P_2 = 0.045 W. To induce exponential motion increases, P_1 was increased to powers of 0.059 W and 0.069 W. Average spring constants for these powers are 4.5×10^{-7} N/m (σ = 2.1 N/m) for P_1 = 0.059 W and 3.4×10^{-7} N/m for P_1 = 0.069 W.

Analysis of results

We compare theoretical predictions to experimental data for 6 μm spheres. Here we plot spring constant as a function of power for three different fiber separations: 68.6 μm, 86.5μm, and 122.0 μm. The lines are plots of Eq. 1 as a function of trapping power (balanced power cases). As can be seen in Fig. 22, there is a direct correlation between power and spring constant values. Also note that the theory curves for separations 68.6 μm and 122.0 μm nearly overlap one another. Markers illustrate experimental spring constant data for three trapping power pairs for the left fiber and right fiber, respectively: P_1 = 0.024 W and P_2 = 0.022 W; P_1 = 0.044 W and P_2 = 0.041 W; and P_1 = 0.049 W and P_2 = 0.045 W.

Fig. 22. Spring constant as a function of trapping power for given fiber separations. Continuous lines are based from the spring constant expression (Eqn. 1) for given powers up to 0.1 W and three fiber separations: 68.8 μm, 86.5 μm, and 122.0 μm. Data points represent experimental data for measured spring constants as a function of trapping power also for the same fiber separations of 68.8 μm, 86.5 μm, and 122.0 μm.

Figure Legend. Fiber separations for the theoretical linear plot: '**Δ**' : 68.8 μm; '*****' : 86.5 μm; '--' : 122.0 μm. Fiber separations for experimental data points: '+' : 68.8 μm, 'x' : 86.5 μm, 'o': 122.0 μm.

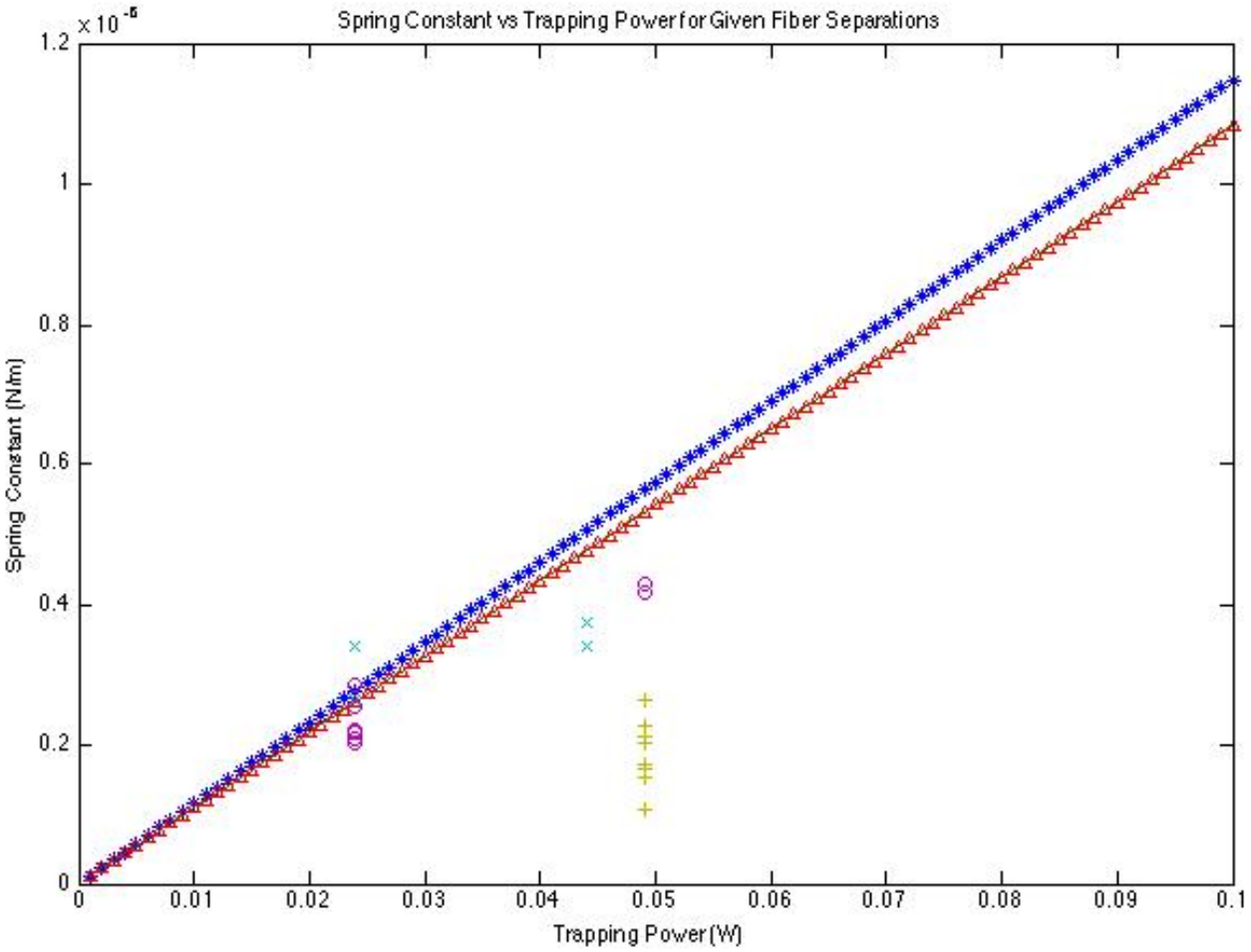

We then statistically compare our data to the mathematical models for spring constants and scattering forces (Eqn. 1 and Eqn. 2). When trapping 6 μm spheres with balanced power settings (~0.047 W) with fiber separations of ~68.8 μm, the average spring constants for decrease curves is 1.87×10^{-7} N/m (-63% error from theoretical); for balanced powers ~0.0425 W with a fiber separation of ~86.5 μm, the average spring constant for decrease curves is 3.57×10^{-7} N/m (-27% error from theoretical); for balanced powers ~0.023 W with fiber separation of 86.5 μm, the average spring constant is 3.01×10^{-7} N/m (+14% from theoretical); for balanced powers ~0.047 W and fiber separation ~122.0 μm, the average spring constant is 4.23×10^{-7} N/m (-16% error from theoretical); and for balanced powers ~0.023 W and fiber separation ~122.0 μm, the average spring constant is 2.31×10^{-7} N/m (-8% error from theoretical).

Measured spring constants are found to increase with higher powers. Experimental spring constants for higher optical power traps are approximately 1.1 to 3 fold times higher than the respective curves for 6 μm spheres trapped in equal power traps. For 10 μm spheres, increase curves have spring constants that are 1.4 to 2 fold times higher than their respective decrease curves.

In some trials the decrease curves have unusually steep initial slopes and do not appear exponential in nature (see Fig. 21). For instance, in these cases with steep curves, about 4 tracking points (i.e. “4 frames”) along the steepest part of the curve are plotted with the particle tracker, rather than the typical average of 10 points tracked. However, keeping in mind our camera system runs at 30 frames/second, our image capability system limits the ability to track moving particles with exponential time constants less than 0.13 s to 0.17 s.

We find that trials with power setting of ~0.023 W with 122.0 ± 2.0 μm fiber separation, and ~0.047 W power for 68.8 ± 1.0 μm fiber separation exhibit approximately identical spring

constant values of $2x10^{-7}$ N/m (see Fig. 22). Although more experimental trials need to be conducted to fully map out the spring constant versus fiber separation curves, shown in Fig. 6, we observe that these identical spring constant values closely reflect curve trends in those figures. Fig. 22 also highlights another finding: it appears that at higher power settings ~0.047 W, the 122.0 μm fiber separation (denoted by 'o') exerts higher spring constant values than the smaller separation of 68.8 μm (denoted by '+'). It is thought that as fiber separation decreases, the trapping volume becomes smaller. Likewise, to some limit, trapping volume increases as fiber separation increases. From Fig. 6 there appears to be an ideal fiber separation of ~100 μm that warrants a maximum spring constant value for the plotted power settings.

We note from Fig. 6b that highly unbalanced curve sets (i.e. $P_1 = 0.069$ W and $P_2 = 0.045$ W, and $P_1 = 0.069$ W and $P_2 = 0.041$ W) can exert maximum spring constants of $6.6x10^{-7}$ N/m at fiber separation ~100 μm. However, our relatively slow camera frame rate of 30 fps does not permit us to measure spring constants higher than ~$3.8x10^{-7}$ N/m for a 6 μm sphere trapped in water, assuming the fastest measurable time constant is approximately 0.13 s to 0.17 s for trapped spheres. Our imaging capabilities also suggest the maximum spring constant we can measure for 10 μm spheres is ~$6.5x10^{-7}$ N/m. As can be seen in Fig. 22 the majority of data points lie below the maximum observable spring constant of $3.8x10^{-7}$ N/m for assays performed with 6μm spheres. To obtain larger time constants, larger microspheres could be utilized, as well as trap in a more viscous fluid.

Our relatively slow image tracking rate gives insight into the low spring constants measured in comparison to theoretical calculations for both microsphere sizes. In some cases, percent error from the theoretical value is relatively high. For instance, the theoretical spring constant for a 10 μm sphere displaced with unbalanced powers ($P_1 = 0.069$ W and $P_2 = 0.045$ W,

increase curve) is 1.21×10^{-6} N/m, giving a percent error of 86% from the measured experimental trials. The theoretical value is much higher than can be measured with our current imaging capabilities.

The microscope set-up is highly sensitive to exterior motion vibrations and audio noise in our laboratory room. This is likely a major source of error that is apparent in some video clips. We have since mechanically stabilized the microscope, which has decreased the observable noise.

Additionally, in our calculations of scattering forces incident on the sphere from the left and right directions, we find that both scattering forces exert approximately the same magnitude on a sphere situated close to the center of the trap. Left and right scattering forces on a 6 μm sphere are within ± 0.2 pN of one another; in contrast, the scattering forces on a 10 μm sphere are ± 1.6 pN with respect to each other. This confirms that the net scattering force acting on a particle in the center of the trapping region counter-act one another; that is, theoretically the net force should be zero. However, in our calculations for scattering forces acting on a particle displaced from the center point are not equal in magnitude. The designated "left scattering force" is consistently shown to be ~8.0 pN higher than the "right scattering force" for displaced 6 μm spheres; for 10 μm spheres the "left scattering force" was an average of ~6.0 pN higher than the "right scattering force." At this point, the net scattering force should be zero again since the sphere is now in equilibrium and no longer accelerating. It is thought that poor fiber alignment or thermal lensing may cause these scattering force offsets to be larger than expected.

It is possible to induce weak trapping of multiple microspheres. Although the SPF 900 optical filter aided in distinguishing between one or more microspheres by eliminating some scattered light, in some instances it is still difficult to determine, for example, if an adjacent

microsphere is weakly trapped almost directly behind the main trapped sphere. In other cases a linear array of ~3 to ~15 microspheres could fall into the trapping region. Note that for these occurrences of multiple trapped spheres, data calculations were not performed, as the output laser light is attenuated differently for an array than a single sphere. This phenomenon of trapped microsphere arrays has been investigated by other research groups [Kawano 2008] and could be one future research endeavor to continue mathematical characterizations of our trap.

In the second part of this investigation, we aim to improve the efficiency of trapping with the XYZ stages. We also look to improve the reproducibility of optical trapping results. As discussed in previous sections, excellent fiber alignment is mandatory for stable traps. With our method of heat-etching channels the diameter of an unjacketed fiber (125 μm) into small cast acrylic plexiglass chips with high-resistive nichrome wires, we demonstrate: 1) the channels serve as feasible waveguides for the optical fibers, thus providing an easy way to achieve fiber alignment; 2) efficient method for getting an array of fibers aligned for array trapping (see Fig. 23).

Fig. 23. Microscope images of trapping in heat-etched channels. **(a)** Representative microscope image of two heat-etched channels with two optical fibers sitting well in the channels. **(b)** A trapped 6 μm sphere between two fibers in a single-channel heat-etched plexiglass chip. Trapping power ~23 mW. **(c)** Two simultaneously trapped 6 μm spheres in 2x2 fiber array scheme. Fibers sit in the two channels of the heat-etched chip. Trapping power ~23 mW from each fiber. **(d)** Four simultaneously trapped 6 μm spheres in 4x4 fiber array scheme. Fibers sit in the four channels of the heat-etched chip. Trapping power ~12 mW from each fiber.

(a)

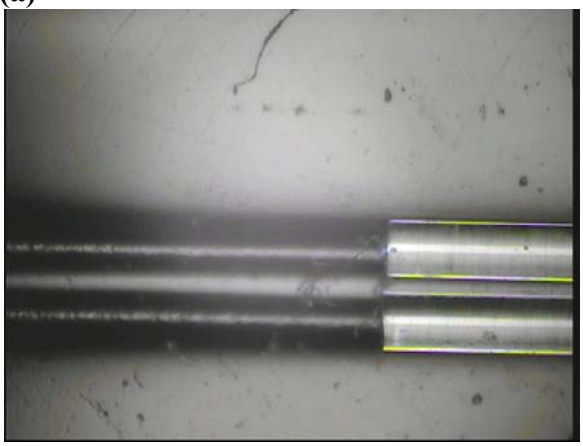

(b)

(c)

(d)

Discussion and conclusions

We have successfully demonstrated and investigated the mechanics of optically trapped microspheres exhibiting overdamped exponential motion through water. Microspheres are trapped in our dual-beam optical trap scheme with XYZ translational stages that align the counter-propagating beams. The forces acting on a trapped particle provide a stable trapping situation that is utilized here to hold and manipulate polystyrene microspheres in water. Thus, this design allows an effective, non-contact method for surveying the trapping forces present in our dual-beam system.

A major limitation of the XYZ translation stage configuration is the tedious nature of manual fiber alignment. Due to the inconsistencies in fiber alignment for each set of experiments, we speculate slight changes in the electric gradient across the trapping region can be affected greatly by micron-sensitive alignment in transverse and angle directions. Later in this investigation we developed a method for easy fiber alignment on plexiglass cast acrylic chips that have provided a major improvement in trapping stable particles in an efficient and consistent manner. We also anticipate this new trapping configuration will decrease the noise observed in position detection plots, decreasing errors in measured spring constants and scattering forces. Furthermore, our technique allows fibers to be superglued into place so that fiber separation is fixed. This improves our ability to quickly perform several sets of measurements; for instance, we can construct various chips of different fixed fiber separations and systematically investigate the effect of a wide spectrum of powers for trapping particles of a given size. The fiber array configuration may offer the opportunity to study several cells simultaneously while exhibiting control of power output for each fiber pair.

Our results explore the pN-force mechanics and behavior of a dual-beam trapping system, and they compare well with published experimental measurements and theoretical calculations from other research groups [Constable 1993 and Jess 2006]. We attribute slight disparities in our data in comparison to published works to different parameters of control: fiber size and mode-field diameter, fiber separation, output power, laser wavelength, and microsphere size. Some of the main findings include: the magnitude of the scattering forces (in the direction of beam propagation) respond linearly to the output power and larger microspheres exert larger time constants (i.e. smaller spring constant values) in comparison to smaller spheres. Furthermore, depending on incident wavelength and output power, there is an ideal fiber separation to achieve maximum spring constant values. In particular, our trap-on-a-chip system is flexible as it permits experimental parameters to be easily altered to obtain desired restoring forces.

Since the first demonstration of optical tweezers by Ashkin [1986], optical manipulation of micron-sized particles has grown into a versatile tool in the physical and life sciences. Integration of optical trapping with modern imaging techniques such as Raman spectroscopy [Jess 2006 and Chan 2009] and total internal reflection fluorescence (TIRF) microscopy [Snijder-Van As 2009] is gaining importance due to the numerous possibilities in biotechnology for this technique. Furthermore, dual-beam optical traps are particularly well suited for integration with microfluidic chips due to the system not requiring bulky, external optical components. Microfluidic-optical trapping combinations have shown promise for various biological and biophysical studies, including single-cell mechanical properties [Cran-McGreehin 2006, Enger 2004, Guck 2005, Lincoln 2007]. We will continue to render our most current

system of trapping on a chip to reflect the need for more cost-effective and easily assembled microfluidic systems.

In the attempt to create a scaled-down approach with greater stability for optically trapping, we have successfully demonstrated trapping on small plexiglass cast acrylic chips (Fig. 23). The trapping occurs within the heat-etched channels, and this method has initially provided a reproducible procedure for creating straight channels. Our scaled-down trap-on-a-chip approach has some benefits including the use of consumable, and inexpensive equipment to trap particles. To date there are no dual-fiber array schemes similar to our configuration employed in current literature. With this chip we have shown we can stably trap 6 μm spheres: one microsphere in a dual-beam trap with ~0.023 W power, two microspheres simultaneously in a 2x2 fiber array with ~0.023 W power, and four simultaneously in a 4x4 fiber array with ~0.012 W power. These microspheres appear to be more stably trapped than spheres trapped with our initial trapping system encompassing XYZ stages.

In the near future we look forward to continuing to calibrate our trapping system with our trap on a chip setup. One first step we will plan to take toward biological studies is trapping cells and conducting viability assays using a near-infrared wavelength (λ = 980 nm) and a range of power settings. We have demonstrated trapping embryonic mouse stem cells with our XYZ translation stage configuration (see Fig. 24), but have not yet conducted cell viability tests.

Fig. 24. Microscope image of mouse embryonic stem cell aggregates trapped with two single mode fibers. Minimum required trapping power ~10 mW with 980 nm light.

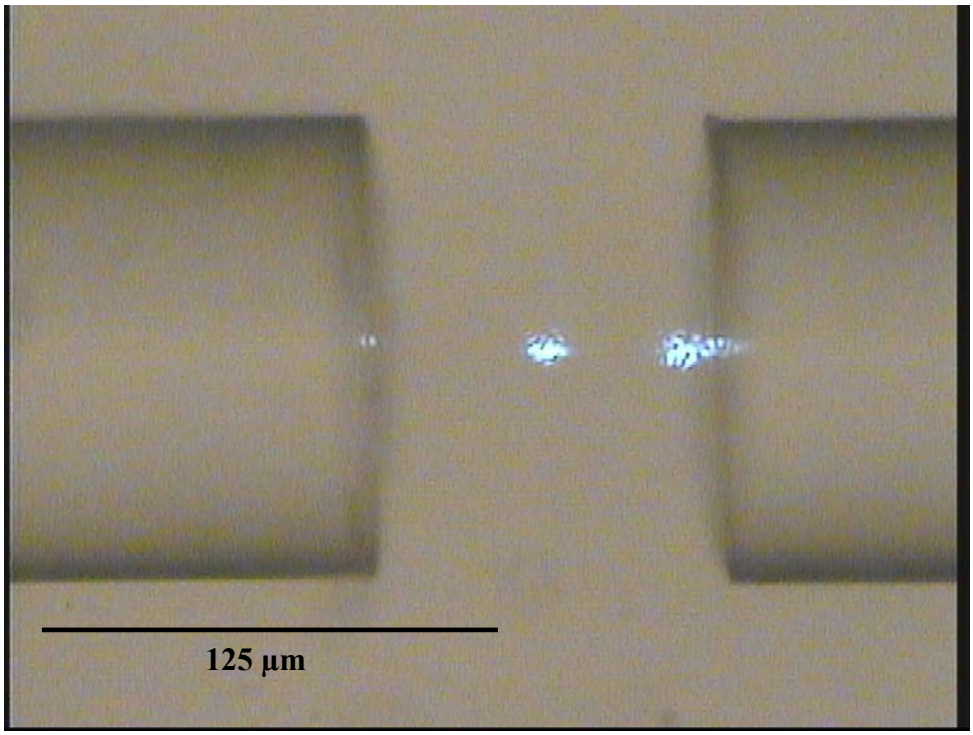

We will optimize power settings to reduce cellular photodamage, and test other wavelengths if necessary. Our new trapping system appears to exhibit much improved fiber alignment, we plan to utilize our new trap-on-a-chip device to continue calibrating our system. We anticipate gathering additional data to expand on the initial results we obtain using the XYZ stage system. With better fiber alignment we anticipate improved results for measured spring constants and scattering forces that more closely reflect theoretical values. Gaining a full understanding of our system capabilities will add value when we pursue biological studies. Since single-cell biophysics is a blossoming field, we foresee numerous opportunities to further optimize our optical trapping tool for biological applications.

References

Applegate, RW, *et al.* 2006. Microfluidic sorting system based on optical waveguide integration and diode laser bar trapping. 6:422-426.

Ashkin, A. 1970. Acceleration and trapping of particles by radiation pressure. Physical Review Letters. 24:156-159.

Ashkin, A. 1983. Stability of radiation-pressure particle traps: an optical Earnshaw theorem. Optics Letters. 8:511-513.

Ashkin, A, *et al.* 1987. Optical trapping and manipulation of single cells using infrared laser beams. Nature. 769-771.

Barth, HG, *et al.* 1984. *Modern Methods of Particle Size Analysis*. Hoboken, NJ:John Wiley & Sons, Inc.

Becker, H and LE Locascio. 2001. Polymer microfluidic devices. Talanta. 56:267-287.

Bohren, CF and DR Huffman. 2004. Absorption and Scattering of Light by Small Particles. Weinheim, Germany:Wiley-VCH.

Blair D and E Dufresne. 2008. "Particle location and tracking tutorial: How to (pre)-track with MATLAB." <http://physics.georgetown.edu/matlab/tutorial.html> (Last accessed 12 June 2009).

Burns, JA, *et al.* 1979. Radiation Forces on Small Particles in the Solar System. Icarus. 40:1-48.

Chan, JW, *et al.* 2009. Label-free separation of human embryonic stem cells and their cardiac derivatives using raman spectroscopy. Analytical Chemistry. 81:1324-1331.

Constable A, *et al.* 1993. Demonstration of a fiber-optical light-force trap. Optics Letters. 18:1867-1869.

Cran-McGreehin S, *et al.* 2006. Integrated monolithic optical manipulation. Lab on a Chip. 6:1122-1124.

Deng, Y, *et al.* 2007. Brownian motion in a modulated optical trap. Journal of Optics A. 9:S256-S263.

Enger J, *et al.*2004. Optical tweezers applied to a microfluidic system. Lab on a Chip. 4:196-200.

Eriksson, E, *et al.* 2007. Optical manipulation and microfluidics for studies of single cell dynamics. Journal of Optics A. 9:S113-S121.

Fowles, GR and GL Cassidy. *2005. Analytical Mechanics*, 5th ed. Belmont, CA: Brooks/Cole.

Grover, SC, *et al.* 2001. Automated single-cell sorting system based on optical trapping. Journal of Biomedical Optics. 6:14-22.

Ghosh, A, *et al.* 2006. Euler buckling-induced folding and rotation of red blood cells in an optical trap. Phys. Biol. 3:67-73.

Guck, J, *et al.* 2005. Optical deformability as an inherent cell marker for testing malignant transformation and metastatic competence. Biophysical Journal. 88:3689-3698.

Hecht, Eugene. 2002. *Optics*, 4th ed. San Francisco: Pearson Addison Wesley.

Irvine, WM. 1965. Light Scattering by Spherical Particles: Radiation Pressure, Asymmetry Factor, and Extinction Cross Section. Journal of the Optical Society of America. 55:16-21.

Jess, PRT, *et al.* 2006. Dual beam fibre trap for Raman micro-spectroscopy of single cells. Optics Express. 14:5779-5791.

Jonasz, M and GR Fournier. 2007. Light Scattering by Particles in Water: Theoretical and Experimental Foundations. Amsterdam:Elsevier Inc.

Kawano, M, *et al.* 2008. Theory of dielectric micro-sphere dynamics in a dual-beam optical trap. Optics Express. 16:9306-9317.

Lincoln, *et al.* 2007. Reconfigurable microfluidic integration of a dual-beam laser trap with biomedical applications. Biomedical Microdevices. 9:703-710.

Malek, CGK. 2006. Laser processing for bio-microfluidics applications (part I). Anal Bioanal Chem. 385:1351-1361.

Mätzler, C. 2002. MATLAB Functions for Mie Scattering and Absorption. Research Report No. 2002-08. Institut für Angewandte Physik, matzler@iap.unibe.ch.

Mätzler, C. 2002. MATLAB Functions for Mie Scattering and Absorption: Version 2. Research Report No. 2002-11. Institut für Angewandte Physik, matzler@iap.unibe.ch.

Mirsaidov, U, *et al*. 2008. Optimal optical trap for bacterial viability. Physical Review E. 78:021910-1-7.

Neuman, KC, *et al.* 1999. Characterization of Photodamage to *Escherichia coli* in Optical Traps. Biophysical Journal. 77:2856-2863.

Park J, *et al*. 2007. Microfabrication-based modulation of embryonic stem cell differentiation. Lab on a chip. 7:1018-1028.

Prasad, PN. 2003. *Introduction to biophotonics.* Hoboken, New Jersey: John Wiley & Sons.

Shah, GA. 1991. Astrophysics and Space Science. Asymmetry Parameter and Efficiency for Radiation Pressure and Scattering of Electromagnetic Radiation by a Very Large Dielectric Particle. 178:251-260.

Singer, W. *et al.* 2003. Self-organized array of regularly spaced microbeads in a fiber-optical trap. Journal of the Optical Society of America B. 20:1568-1574.

Snijder-Van As, MI, *et al.* 2009. A hybrid total internal reflection fluorescence and optical tweezers microscope to study cell adhesion and membrane protein dynamics of single living cells. Journal of Microscopy. 233:84-92.

Thomas, ME. 2006. *Optical Propagation in Linear Media: Atmospheric Gases and Particles, Solid-State Components, and Water.* New York City: Oxford University Press, Inc.

Van de Hulst, HC. 1981. Light Scattering by Small Particles. Mineola, NY:Dover.

Wang, MM, *et al*. 2005. Microfluidic sorting of mammalian cells by optical force switching. Nature Biotechnology. 23:83-87.

Wei, MW, *et al.* 2006. Three-dimensional optical force field on a Chinese hamster ovary cell in a fiber-optical dual-beam trap. Optics Express. 14:3056-3064.

Appendix

MATLAB .mpg video particle tracking program, Blair and Dufresne (2008)

```
%MPG video tracking program for trapped microspheres and plot position as
function of time
%Based from Blair and Dufresne (2008)

%clean up the work environment
clear all
close all

%begin and end time for processing the data in seconds
stime=1;
ftime=26;

%approximate size of the particle in pixels USE AN ODD NUMBER
ptclsize=11;

%needs to be figured out during trial run...set to a large number and see
%what is the size of xcenters to get the real number
nframes=749;

%loads up the video named movie.mpg
vid=mmread('movie2.mpg',[],[stime ftime],false,true);

%loop through the individual pictures to get the position of the particle
for p=1:nframes;

% gets the frames from bizarre mmread format into the right format (height X
width array of unit8), scale and contrast: find "cdata" one frame
aa = vid.frames(p).cdata;
tim(p)=vid.times(p);
aa=255-aa; % look at negative of image
a=aa(:,:,3); % look only at blue part of image
a=255-a; % make it a positive image again
b = bpass(a,1,50); %do a bandpass filter (I used 0,50 and it worked well...but
you might need to change these)
thresh = max(max(b))*.95; %pick the threshold (I used 95% and that was fine)
```

```
pk = pkfnd(b,thresh,ptclsize) %locate the peak for an object about 31 pixels
wide

cnt = cntrd(b,pk,ptclsize+10) %centroid of the found peak

%insert the results into output data arrays
indx(p)=p;
xcenters(p)=cnt(1);
ycenters(p)=cnt(2);

end

%plot the results
figure;
colormap('gray'), imagesc(b);
 figure;
 plot(tim,xcenters,'o');

%nice labels on the plots
xlabel('Image Number')
ylabel('X-Position on Image (pixels)')
title('Plot of Pixel X-Position versus Time (s)','FontSize',14)

figure;
plot(tim,ycenters);
xlabel('Time (s)')
ylabel('Y-Position on Image (pixels)')
title('Plot of Pixel Y-Postition versus Time (s)','FontSize',14)
%csvwrite('movie2_time.csv',transpose(tim));
%csvwrite('movie2xpos_1-26s.csv',transpose(xcenters));
%csvwrite('movie2ypos_1-26s.csv',transpose(ycenters));
```

Mie scattering coefficient programs (Mätzler 2002, with minor modifications by Tessa Piñón)

#a) This program utilizes a_n, b_n, c_n, and d_n to calculate scattering coefficient values

```
%Mie scattering coefficient program calculations are from Christian Matzler's
"MATLAB
%Functions for Mie Scattering and Absorption" paper-Research Report no.
%2002-08. June 2002.

%I have done minor modifications to Mätzler's original code to fit the
%parameters of our experiment


function result = tessamie_abcd6um(m, x)

%For 6.0 um diameter polystyrene microsphere
r = 3.0E-6;
x = (2*pi*r*1.33)/980E-9;
m = 1.59/1.33;


%Statement below satisfies requirement for an and bn mie coefficients: that
%they are 0 for x = 0 and are continuous functions of x. They are 0 for
%m=1 and continuous functions of m [Van de Hulst p.136].


%if x==0                  % To avoid a singularity at x=0
    %result=[0 0 0 0 0 1.5];
    % This is the normal situation

nmax=round(2+x+4*x.^(1/3));  %Termination for n value [Bohren & Huffman]
n=(1:nmax);
nu = (n+0.5); %denotes half-integral order
z=m.*x; %given argument
m2=m.*m;

%Spherical Bessel functions defined-(Bohren & Huffman, p. 86)
sqx= sqrt(0.5*pi./x); sqz= sqrt(0.5*pi./z);


bx = besselj(nu, x).*sqx;
bz = besselj(nu, z).*sqz;

yx = bessely(nu, x).*sqx;

hx = bx+i*yx;

b1x=[sin(x)/x, bx(1:nmax-1)];
b1z=[sin(z)/z, bz(1:nmax-1)];

y1x=[-cos(x)/x, yx(1:nmax-1)];

h1x= b1x+i*y1x;

ax = x.*b1x-n.*bx;
az = z.*b1z-n.*bz;

ahx= x.*h1x-n.*hx;

an = (m2.*bz.*ax-bx.*az)./(m2.*bz.*ahx-hx.*az);
bn = (bz.*ax-bx.*az)./(bz.*ahx-hx.*az);
cn = (bx.*ahx-hx.*ax)./(bz.*ahx-hx.*az);
```

```
dn = m.*(bx.*ahx-hx.*ax)./(m2.*bz.*ahx-hx.*az);
result=[an; bn; cn; dn];



    n1=nmax-1;
    n=(1:nmax);cn=2*n+1; c1n=n.*(n+2)./(n+1); c2n=cn./n./(n+1);
    x2=x.*x;
    f=tessamie_ab6um(m,x);          %an = first row, bn = second row
    anp=(real(f(1,:))); anpp=(imag(f(1,:)));
    bnp=(real(f(2,:))); bnpp=(imag(f(2,:)));
    g1(1:4,nmax)=[0; 0; 0; 0]; % displaced numbers used for
    g1(1,1:n1)=anp(2:nmax);    % [asymmetry parameter, Bohren & Huffmaan, p.
120]
    g1(2,1:n1)=anpp(2:nmax);
    g1(3,1:n1)=bnp(2:nmax);
    g1(4,1:n1)=bnpp(2:nmax);

    % Extinction Coefficient
    dn=cn.*(anp+bnp);
    q=sum(dn);
    qext=2*q/x2;

    % Scattering Coefficient
    en=cn.*(anp.*anp+anpp.*anpp+bnp.*bnp+bnpp.*bnpp);
    q=sum(en);
    qsca=2*q/x2;
    qabs=qext-qsca;

    % Backscattering -- [Bohren & Huffman, p. 122]
    fn=(f(1,:)-f(2,:)).*cn;
    gn=(-1).^n;
    f(3,:)=fn.*gn;
    q=sum(f(3,:));
    qb=q*q'/x2;

    asy1=c1n.*(anp.*g1(1,:)+anpp.*g1(2,:)+bnp.*g1(3,:)+bnpp.*g1(4,:));
    asy2=c2n.*(anp.*bnp+anpp.*bnpp);
    asy=4/x2*sum(asy1+asy2)/qsca;
    qratio=qb/qsca;


    qpr = qext-(asy*qsca);


    Table = [qext',  qsca',          qabs',                              qb',
asy'        qratio     qpr'];
    disp('')
    disp('For 6.0um diameter dielectric polystyrene microsphere')
    disp('     Qext       Qsca        Qabs    Qb   <cos(theta)> Qb/Qsca
Qpr')
    disp('')
    disp(Table)
    disp('')
```

#b)

```
function result = tessamie_ab6um(m,x)

% Computes a matrix of Mie Coefficients, an, bn,
% of orders n=1 to nmax, for given complex refractive-index
```

```
% ratio m=m'+im" and size parameter x=k0*a where k0= wave number in ambient
% medium for spheres of radius a;
% Eq. (4.88) of Bohren and Huffman (1983)
% using the recurrence relation (4.89) for Dn on p. 127 and
% starting conditions as described in Appendix A.
% C. Mätzler, July 2002

r = 3.0E-6;
x = (2*pi*r*1.33)/980E-9;
m = 1.59/1.33;


z=m.*x;
nmax=round(2+x+4*x.^(1/3));
nmx=round(max(nmax,abs(z))+16);

n=(1:nmax); nu = (n+0.5);

sx=sqrt(0.5*pi*x);

px=sx.*besselj(nu,x);
p1x=[sin(x), px(1:nmax-1)];


chx=-sx.*bessely(nu,x);

ch1x=[cos(x), chx(1:nmax-1)];

gsx=px-i*chx; gs1x=p1x-i*ch1x;

dnx(nmx)=0+0i;

for j=nmx:-1:2      % Computation of Dn(z) according to (4.89) of Bohren
& Huffman (1983)
    dnx(j-1)=j./z-1/(dnx(j)+j./z);
end;
dn=dnx(n);          % Dn(z), n=1 to nmax
da=dn./m+n./x;
db=m.*dn+n./x;

an=(da.*px-p1x)./(da.*gsx-gs1x);
bn=(db.*px-p1x)./(db.*gsx-gs1x);

result=[an; bn];
```

MATLAB spring constant program, Eqn. 1 as referenced in text. Program based from Constable (1993).

```
%This program calculates the spring constant "k" (theoretical) for a
%trapped 10um diameter polystyrene microsphere in water. This program
%is based from Constable's (1993) article--Eq. 2.

%Qpr value calculated using Mätzler's Mie scattering coefficient MATLAB
%program (separate from this code)


%For 10.0 um diameter polystyrene microspheres
a = (2*(5.0E-6)^2)/3E8; %Incident cross-sectional area
q = 0.2013; %Qpr
w = 5E-6;   %Gaussian beam waist
```

```
n = 980E-9; %Laser wavelength
d = (pi*(w)^2)/n;


%Output power (W) of counter-propagating beams
p1 = 69E-3; %Left beam
p2 = 45E-3; %Right beam

s = 77E-6;  %Fiber separation

k1 = (16*(pi^2)*a*s);
k2 = (p1*q*(w^2))/((n^2)*((s^2)+(4*(d^2)))^2);
k3 = (p2*q*(w^2))/((n^2)*((s^2)+(4*(d^2)))^2);
k = k1*(k2+k3) %Theoretical spring constant
```

MATLAB Scattering Force Program, Eqn. 2 as Referenced in Text. Program based from Constable (1993).

```
%This program calculates the net scattering force on a trapped 10um
% sphere in water. This program is based from Constable's (1993)
%article--Eqn. 1.

%Qpr value calculated using Matzler's Mie scattering coefficent MATLAB
%program (separate from this code)



%For 10.0 um diameter polystyrene microsphere
a = (2*(5.0E-6)^2)/3E8; %Incident cross-sectional area
q = 0.2013; %Qpr (radiation pressure coefficient)
w = 5E-6; %Gaussian beam waist
n = 980E-9; %Laser wavelength
d = (pi*(w)^2)/n;
```

```
s = 77.0E-6;

%Output power (W) of counter-propagating beams
p1 = 69E-3; %Left beam
p2 = 45E-3; %Right beam

z = 37E-6; %Displacement of microsphere relative to trap center

f1 = ((a*p1*q)/(w^2))/(1+((d^-2)*((s/2)+z)^2)); %Left scattering force
f2 = ((a*p2*q)/(w^2))/(1+((d^-2)*((s/2)-z)^2)); %Right scattering force

f = f1
f = f2
f = f1-f2 %Net scattering force
```

Raw data of experimental trapping data conducted by T. Piñón. The following charts only include experimental runs when powers are offset (i.e. microsphere is displaced from trap).

7/1/2008 Data (Movie 1): _scope_20080701_142659.mpg						
Experimental Parameters:	**Exponential Curve**	**Time Constant (τ)--s**	**Spring Constant (κ)--N/m**	**Displacement from Center (μm)**	**Left Scattering Force (pN)**	**Right Scattering Force (pN)**
Bead diameter: 6 μm	Increase 1	0.08	6.29E-07	11.6	33.5	25.3
Laser 1: 44 mW <--> 69 mW	Decrease 1	0.148	3.40E-07	3.68	23.3	23.5
Laser 2: 41 mW	Increase 2	0.045	1.12E-06	11.6	33.5	25.3
Fiber Separation: 86.5 μm	Decrease 2	0.135	3.73E-07	3.68	23.3	23.5
Time Frame Analyzed: 18-48s						
Qpr = 0.2968 (from Matzler Program)				**Theoretical κ for Decrease (N/m)**	**Theoretical κ for Increase (N/m)**	
Scaling: 221 pix = 125 μm		Increase Ave (τ): 0.063 s	Increase Ave κ: 8.75E-7 N/m	--------	6.33E-07	**% Error: 38%**
153 pix = 86.5 μm		Decrease Ave (τ): 0.142 s	Decrease Ave κ: 3.57E-7 N/m	4.89E-07	-------	**% Error: 27%**
Sphere initial position: 6.5 pix from center = 3.68 μm						
Comments: Increase curves are really steep (don't look exponential)						

7/1/2008 Data (Movie 2): _scope_20080701_143138.mpg						
Experimental Parameters:	**Exponential Curve**	**Time Constant (τ)--s**	**Spring Constant (κ)--N/m**	**Displacement from Center (μm)**	**Left Scattering Force (pN)**	**Right Scattering Force (pN)**
Bead diameter: 6μm	Increase 1	0.126	3.99E-07	18.4	21.9	14.3
Laser 1: 24 mW <--> 49 mW	Decrease 1	0.148	3.40E-07	3.11	12.8	12.5
Laser 2: 22 mW	Increase 2	0.116	4.34E-07	18.4	21.9	14.3
Fiber Separation: 86.5 μm	Decrease 2	0.192	2.62E-07	3.11	12.8	12.5
Time Frame Analyzed: 12-42s						
Qpr = 0.2968 (from Matzler Program)				**Theoretical κ for Decrease (N/m)**	**Theoretical κ for Increase (N/m)**	
		Increase Ave (τ): 0.121 s	Increase Ave κ: 4.17E-7 N/m	-------	4.09E-07	**% Error: 2%**
Scaling: 221 pix = 125 μm		Decrease Ave (τ): 0.170 s	Decrease Ave κ: 3.01E-7 N/m	2.65E-07	--------	**% Error: 14%**
153 pix = 86.5 μm						
Sphere initial position: 5.5 pix from center = 3.11 μm						
Comments:						

7/1/2008 Data (Movie 3): _scope_20080701_143427.mpg						
Experimental Parameters:	**Exponential Curve**	**Time Constant (τ)--s**	**Spring Constant (κ)--N/m**	**Displacement from Center (μm)**	**Left Scattering Force (pN)**	**Right Scattering Force (pN)**
Bead diameter: 6μm	Increase 1	0.234 s	2.07E-7 N/m	45.8	9.24	2.85
Laser 1: 4 mW <--> 29 mW						
Laser 2: 4 mW				**Theoretical Scattering Force for Decrease (N/m)**	**Theoretical κ for Increase (N/m)**	
Fiber Separation: 86.5 μm				N/A	1.90E-07	
Time Frame Analyzed: 22-26s					**% Error: 9%**	
Qpr = 0.2968 (from Matzler Program)						
Scaling: 221 pix = 125 μm						
153 pix = 86.5 μm						
Sphere initial position: 1.5 pix from center = 0.85 μm						
Comments: Too large of a power change--sphere moved all the way to the end of the fiber, but curve looks good; 4 mW of power is most likely lower than minimum power required for trapping						

9/19/2008 Data (Movie 2): _scope_20080919_160325.mpg						
Experimental Parameters:	**Exponential Curve**	**Time Constant (τ)--s**	**Spring Constant (κ)--N/m**	**Displacement from Center (μm)**	**Left Scattering Force (pN)**	**Right Scattering Force (pN)**
Bead diameter: 6μm	Increase 1	0.252	2.00E-07	14.4	25.6	23.6
Laser 1: 49mW <--> 69 mW	Decrease 1	0.117	4.30E-07	3.06	20.9	20.7
Laser 2: 45 mW	Increase 2	0.234	2.15E-07	14.4	25.6	23.6
Fiber Separation: 125 μm	Decrease 2	0.121	4.16E-07	3.06	20.9	20.7
Time Frame Analyzed: 1-37s	Increase 3	0.225	2.24E-07	14.4	25.6	23.6
Qpr = 0.2968 (from Matzler Program)						
				Theoretical κ for Decrease (N/m)	**Theoretical κ for Increase (N/m)**	
Scaling: 143 pix = 125 μm		Increase Ave (τ): 0.237 s	Increase Ave κ: 2.13E-7 N/m	-------	6.11E-07	**% Error: 66%**
Sphere initial position: 3.5 pix from center = 3.06 μm		Decrease Ave (τ): 0.119 s	Decrease Ave κ: 4.23E-7 N/m	5.04E-07	-------	**% Error: 16%**
Comments: Data is noisy--time constant values not consistent with data trend						

9/19/2008 Data (Movie 3): _scope_20080919_160751.mpg						
Experimental Parameters:	**Exponential Curve**	**Time Constant (τ)--s**	**Spring Constant (κ)--N/m**	**Displacement from Center (μm)**	**Left Scattering Force (pN)**	**Right Scattering Force (pN)**
Bead diameter: 6μm	Increase 1	0.133	3.78E-07	16.6	15.1	12
Laser 1: 24mW <--> 41 mW	Decrease 1	0.199	2.53E-07	4.37	10.3	10.5
Laser 2: 22 mW	Increase 2	0.138	3.65E-07	16.6	15.1	12
Fiber Separation: 122 μm	Decrease 2	0.233	2.16E-07	4.37	10.3	10.5
Time Frame Analyzed: 1-31s						
Qpr = 0.2968 (from Matzler Program)				**Theoretical κ--Decrease (N/m)**	**Theoretical κ--Increase (N/m)**	
		Increase Ave (τ): 0.136 s	Increase Ave κ: 3.72E-7 N/m	------	3.42E-07	**% Error: 9%**
Scaling: 143 pix = 125 μm		Decrease Ave (τ): 0.169 s	Decrease Ave κ: 2.35E-7 N/m	2.50E-07	-------	**% Error: 6%**
140 pix = 122 μm						
Sphere initial position: 5 pix from center = 4.37 μm						
Comments: Modulation is odd--looks like Laser 2 is being modulated instead? (or Laser 1 decreased?), difficult to tell, so data may be off						

9/19/2008 Data (Movie 6): _scope_20080919_162245.mpg						
Experimental Parameters:	**Exponential Curve**	**Time Constant (τ)--s**	**Spring Constant (κ)--N/m**	**Displacement from Center (μm)**	**Left Scattering Force (pN)**	**Right Scattering Force (pN)**
Bead diameter: 6μm	Increase 1	0.205	2.46E-07	20.1	17.2	12.4
Laser 1: 24mW <--> 49 mW	Decrease 1	0.251	2.01E-07	4.37	10.3	10.5
Laser 2: 22 mW	Increase 2	0.112	4.49E-07	20.1	17.2	12.4
Fiber Separation: 122 μm	Decrease 2	0.176	2.86E-07	4.37	10.3	10.5
Time Frame Analyzed: 1-31s						
Qpr = 0.2968 (from Matzler Program)				**Theoretical κ--Decrease (N/m)**	**Theoretical κ--Increase (N/m)**	
		Increase Ave (τ): 0.159 s	Increase Ave κ: 3.48E-7 N/m	--------	3.85E-07	**% Error: 10%**
Scaling: 143 pix = 125 μm		Decrease Ave (τ): 0.214 s	Decrease Ave κ: 2.44E-7 N/m	2.50E-07	------	**% Error: 2%**
140 pix = 122 μm						
Sphere initial position 5 pix from center = 4.37 μm						
Comments: 2 beads might be trapped						

9/19/2008 Data (Movie 7): _scope_20080919_162422.mpg						
Experimental Parameters:	**Exponential Curve**	**Time Constant (τ)--s**	**Spring Constant (κ)--N/m**	**Displacement from Center (μm)**	**Left Scattering Force (pN)**	**Right Scattering Force (pN)**
Bead diameter: 6μm	Increase 1	0.065	7.74E-07	20.5	17.4	12.6
Laser 1: 24mW <--> 49 mW	Decrease 1	0.242	2.08E-07	3.06	10.6	10.4
Laser 2: 22 mW	Increase 2	0.099	5.08E-07	20.5	17.4	12.6
Fiber Separation: 120 μm	Decrease 2	0.23	2.19E-07	3.06	10.6	10.4
Time Frame Analyzed: 8-38s						
Qpr = 0.2968 (from Matzler Program)				**Theoretical κ--Decrease (N/m)**	**Theoretical κ--Increase (N/m)**	
		Increase Ave (τ): 0.082 s	Increase Ave κ: 6.41E-7 N/m	--------	3.88E-07	**% Error: 65%**
Scaling: 143 pix = 125 μm		Decrease Ave (τ): 0.236 s	Decrease Ave κ: 2.14E-7 N/m	2.51E-07	-------	**% Error: 15%**
137 pix = 120 μm						
Sphere initial position: 3.5 pix from center = 3.06 μm						
Comments: Looks like there are 2 beads trapped						

9/20/2008 Data (Movie 6): _scope_20080920_195859.mpg						
Experimental Parameters:	**Exponential Curve**	**Time Constant (τ)--s**	**Spring Constant (κ)--N/m**	**Displacement from Center (μm)**	**Left Scattering Force (pN)**	**Right Scattering Force (pN)**
Bead diameter: 6μm	Increase 1	0.173	2.91E-07	12.3	41.7	30.1
Laser 1: 49mW <--> 79 mW	Decrease 1	Too noisy	Too noisy	N/A	N/A	N/A
Laser 2: 45 mW	Increase 2	0.211	2.39E-07	13.5	41.7	30.1
Fiber Separation: 67.9 μm						
Time Frame Analyzed: 12-42s				**Theoretical κ-- Decrease (N/m)**	**Theoretical κ-- Increase (N/m)**	
Qpr = 0.2968 (from Matzler Program)		Increase Ave (τ): 0.192 s	Increase Ave κ: 2.65E-7 N/m	-------	6.71E-07	**% Error: 61%**
Scaling: 208 pix = 125 μm		Decrease Ave (τ): N/A	Decrease Ave κ: N/A	5.09E-07	------	**% Error: N/A**
113 pix = 67.9 μm						
Sphere initial position: 8.5 pix from center = 5.11 μm						
Comments: Data plots were extremely noisy-Decreases could not be analyzed						

9/20/2008 Data (Movie 7): _scope_20080920_200117.mpg						
Experimental Parameters:	**Exponential Curve**	**Time Constant (τ)--s**	**Spring Constant (κ)--N/m**	**Displacement from Center (μm)**	**Left Scattering Force (pN)**	**Right Scattering Force (pN)**
Bead diameter: 6μm	Increase 1	0.103	4.89E-07	10	37.6	29.4
Laser 1: 49mW <--> 69 mW	Decrease 1	0.224	2.25E-07	3.94	28.4	28
Laser 2: 45 mW	Increase 2	0.172	2.93E-07	10	37.6	29.4
Fiber Separation: 68.6 μm	Decrease 2	0.192	2.62E-07	3.94	28.4	28
Time Frame Analyzed: 13-43s						
Qpr = 0.2968 (from Matzler Program)				**Theoretical κ-- Decrease (N/m)**	**Theoretical κ-- Increase (N/m)**	
		Increase Ave (τ): 0.138 s	Increase Ave κ: 3.91E-7 N/m	-----	6.20E-07	**%Error: 37%**
Scaling: 206 pix = 125 μm		Decrease Ave (τ): 0.208	Decrease Ave κ: 2.44E-7 N/m	5.11E-07	-------	**%Error: 52%**
113 pix = 68.6 μm						
Sphere initial position 6.5 pix from center = 3.94 μm						
Comments: Noisy data						

9/20/2008 Data (Movie 9): _scope_20080920_200458.mpg						
Experimental Parameters:	**Exponential Curve**	**Time Constant (τ)--s**	**Spring Constant (κ)--N/m**	**Displacement from Center (μm)**	**Left Scattering Force (pN)**	**Right Scattering Force (pN)**
Bead diameter: 6μm	Increase 1	0.237	2.12E-07	13	41.7	29.9
Laser 1: 49 mW <--> 79 mW	Decrease 1	0.292	1.72E-07	5.09	28.1	28.3
Laser 2: 45 mW	Decrease 2	0.251	2.01E-07	5.09	28.1	28.3
Fiber Separation: 68.8 μm						
Time Frame Analyzed: 1-31s				**Theoretical κ--Decrease (N/m)**	**Theoretical κ--Increase (N/m)**	
Qpr = 0.2968 (from Matzler Program)		Increase Ave (τ): 0.237s	Increase Ave κ: 2.12E-7 N/m	------	6.75E-07	**% Error: 69%**
Scaling: 381 pix = 125 μm		Decrease Ave (τ): 0272s	Decrease Ave κ: 1.87E-7 N/m	5.11E-07	--------	**% Error: 63%**
209 pix = 68.8 μm						
Sphere initial position 15.5 pix from center = 5.09 μm						
Comments: Noisy data						

9/20/2008 Data (Movie 10): _scope_20080920_200638.mpg						
Experimental Parameters:	**Exponential Curve**	**Time Constant (τ)--s**	**Spring Constant (κ)--N/m**	**Displacement from Center (μm)**	**Left Scattering Force (pN)**	**Right Scattering Force (pN)**
Bead diameter: 6μm	Increase 1	0.204	2.47E-07	15.3	48.1	30.3
Laser 1: 49 mW <--> 94 mW	Decrease 1	0.332	1.52E-07	3.65	28.4	27.8
Laser 2: 45 mW	Decrease 2	0.237	2.12E-07	3.65	28.4	27.8
Fiber Separation: 69.6 μm						
Time Frame Analyzed: 1-31s				**Theoretical κ--Decrease (N/m)**	**Theoretical κ--Increase (N/m)**	
Qpr = 0.2968 (from Matzler Program)		Increase Ave (τ): 0.204 s	Increase Ave κ: 2.74E-7 N/m	-------	7.60E-07	**% Error: 64%**
Scaling: 377 pix = 125 μm		Decrease Ave (τ): 0.285 s	Decrease Ave κ: 1.82E-7 N/m	5.14E-07	--------	**% Error: 65%**
210 pix = 69.6 μm						
Sphere initial position 11.0 pix from center = 3.65 μm						
Comments: Noisy data						

9/20/2008 Data (Movie 12): _scope_20080920_201004.mpg						
Experimental Parameters:	**Exponential Curve**	**Time Constant (τ)--s**	**Spring Constant (κ)--N/m**	**Displacement from Center (μm)**	**Left Scattering Force (pN)**	**Right Scattering Force (pN)**
Bead diameter: 6μm	Increase 1	0.2	2.52E-07	17.7	49.7	30.8
Laser 1: 49 mW <--> 99 mW	Decrease 1	0.478	1.05E-07	5.77	28	28.5
Laser 2: 45 mW	Increase 2	0.159	3.17E-07	17.7	49.7	30.8
Fiber Separation: 68.3 μm	Decrease 2	0.304	1.66E-07	5.77	28	28.5
Time Frame Analyzed: 1-31s						
Qpr = 0.2968 (from Matzler				**Theoretical κ-- Decrease (N/m)**	**Theoretical κ-- Increase (N/m)**	
Program)		Increase Ave (τ): 0.180 s	Increase Ave κ: 2.85E-7 N/m	------	7.81E-07	**% Error: 64%**
Scaling: 379 pix = 125 μm		Decrease Ave (τ): 0.391 s	Decrease Ave κ: 1.36E-7 N/m	5.10E-07	--------	**% Error: 73%**
207 pix = 68.3 μm						
Sphere initial position: 17.5 pix from center = 5.77 μm						
Comments: Noisy decrease curves						

9/23/2008 Data (Movie 2): _scope_20080923_192424.mpg						
Experimental Parameters:	**Exponential Curve**	**Time Constant (τ)--s**	**Spring Constant (κ)--N/m**	**Displacement from Center (μm)**	**Left Scattering Force (pN)**	**Right Scattering Force (pN)**
Bead diameter: 10 μm	Increase 1	0.236	3.55E-07	37	49.1	60.4
Laser 1: 49 mW <--> 69 mW	Decrease 1	0.511	1.64E-07	5.72	50.4	51.7
Laser 2: 45 mW	Increase 2	0.258	3.25E-07	37	49.1	60.4
Fiber Separation: 77.0 μm	Decrease 2	0.49	1.71E-07	5.72	50.4	51.7
Time Frame Analyzed: 1-37s						
Qpr = 0.2013 (from Matzler Program)				**Theoretical κ-- Decrease (N/m)**	**Theoretical κ-- Increase (N/m)**	
		Increase Ave (τ): 0.247 s	Increase Ave κ: 3.40E-7 N/m	------	1.21E-06	**%Error: 86%**
Scaling: 164 pix = 125 μm		Decrease Ave (τ): 0.501 s	Decrease Ave κ: 1.68E-7 N/m	9.98E-07	-------	**%Error: 83%**
101 pix = 77.0 μm						
Sphere initial position 7.5 pix from center = 5.72 μm						
Comments:						

9/23/2008 Data (Movie 3): _scope_20080923_192624.mpg						
Experimental Parameters:	**Exponential Curve**	**Time Constant (τ)--s**	**Spring Constant (κ)--N/m**	**Displacement from Center (μm)**	**Left Scattering Force (pN)**	**Right Scattering Force (pN)**
Bead diameter: 10 μm	Increase 1	0.133	6.31E-07	28.6	50.5	59.5
Laser 1: 49 mW <--> 64 mW						
Laser 2: 45 mW						
Fiber Separation: 77.0 μm				**Theoretical κ-- Decrease (N/m)**	**Theoretical κ-- Increase (N/m)**	
Time Frame Analyzed: 15-45s				9.98E-07	1.16E-06	
Qpr = 0.2013 (from Matzler				**% Error: N/A**	**%Error: 46%**	
Scaling: 164 pix = 125 μm						
101 μm = 77 um						
Sphere initial position: 4.5 pix from center = 3.43 um						
Comments: Data very noisy and not exponential--only one increase curve was decent (fibers misaligned)						

9/23/2008 Data (Movie 4): _scope_20080923_192831.mpg						
Experimental Parameters:	**Exponential Curve**	**Time Constant (τ)--s**	**Spring Constant (κ)--N/m**	**Displacement from Center (μm)**	**Left Scattering Force (pN)**	**Right Scattering Force (pN)**
Bead diameter: 10 μm	Increase 1	0.354	2.37E-07	18.7	52.5	56.9
Laser 1: 49 mW <--> 59 mW	Decrease 1	0.493	1.70E-07	3.43	51.6	50.7
Laser 2: 45 mW						
Fiber Separation: 77.0 μm				**Theoretical κ-- Decrease (N/m)**	**Theoretical κ-- Increase (N/m)**	
Time Frame Analyzed: 15-45s				9.98E-07	1.10E-06	
Qpr = 0.2013 (from Matzler Program)				**% Error: 84%**	**% Error: 68%**	
Scaling: 164 pix = 125 μm						
101 pix = 77.0 μm						
Sphere initial position: 4.5 pix from center = 3.43 μm						
Comments: Data was really noisy for other curves and could not analyze them						

9/23/2008 Data (Movie 5): _scope_20080923_193055.mpg						
Experimental Parameters:	**Exponential Curve**	**Time Constant (τ)--s**	**Spring Constant (κ)--N/m**	**Displacement from Center (μm)**	**Left Scattering Force (pN)**	**Right Scattering Force (pN)**
Bead diameter: 10 μm	Increase 1	0.185	4.53E-07	18.7	52.5	56.9
Laser 1: 49 mW <--> 59 mW	Decrease 1	0.259	3.24E-07	3.43	51.6	50.7
Laser 2: 45 mW	Increase 2	0.126	6.66E-07	18.7	52.5	56.9
Fiber Separation: 77.0 μm	Decrease 2	0.332	2.53E-07	3.43	51.6	50.7
Time Frame Analyzed: 15-45s						
Qpr = 0.2013 (from Matzler Program)				**Theoretical κ--Decrease (N/m)**	**Theoretical κ--Increase (N/m)**	
Scaling: 164 pix = 125 μm		Increase Ave (τ): 0.156 s	Increase Ave κ: 5.60E-7 N/m	-------	1.10E-06	**%Error: 49%**
101 pix = 77 μm		Decrease Ave (τ): 0.296 s	Decrease Ave κ: 2.89E-7 N/m	9.98E-07	------	**%Error: 71%**
Sphere initial position: 4.5 pix from center = 3.43 μm						
Comments: Curves were not exponential (too steep)						

9/23/2008 Data (Movie 7): _scope_20080923_193517.mpg						
Experimental Parameters:	**Exponential Curve**	**Time Constant (τ)--s**	**Spring Constant (κ)--N/m**	**Displacement from Center (μm)**	**Left Scattering Force (pN)**	**Right Scattering Force (pN)**
Bead diameter: 10 μm	Increase 1	Not exponential	N/A	N/A		
Laser 1: 49 mW <--> 59 mW	Decrease 1	0.408	2.06E-07	1.03	53.6	50.2
Laser 2: 45 mW	Increase 2	Not exponential	N/A	N/A		
Fiber Separation: 74.2 μm	Decrease 2	0.38	2.21E-07	1.03	53.6	50.2
Time Frame Analyzed: 10-40s						
Qpr = 0.2013 (from Matzler Program)				**Theoretical κ--Decrease (N/m)**	**Theoretical κ--Increase (N/m)**	
		Increase Ave (τ): N/A	Increase Ave κ: N/A	-----	1.09E-06	**% Error: N/A**
Scaling: 364 pix = 125 μm		Decrease Ave (τ): 0.394	Decrease Ave κ: 2.14E-7	9.88E-07	-----	**%Error: 78%**
216 pix = 74.2 μm						
Sphere initial position: 3.0 pix from center = 1.03 μm						
Comments: Increase curves were not exponential						